Cellular/Molecular

Extrasynaptic $GABA_A$ Receptors Couple Presynaptic Activity to Postsynaptic Inhibition in the Somatosensory Thalamus

Murray B. Herd, Adam R. Brown, Jeremy J. Lambert,* and Delia Belelli*

Division of Neuroscience, Medical Research Institute, University of Dundee, Ninewells Hospital and Medical School, Dundee, DD1 9SY, United Kingdom

Thalamocortical circuits govern cognitive, sensorimotor, and sleep-related network processes, and generate pathological activities during absence epilepsy. Inhibitory control of thalamocortical (TC) relay neurons is partially mediated by GABA released from neurons of the thalamic reticular nucleus (nRT), acting predominantly via synaptic $\alpha1\beta2\gamma2$ $GABA_A$ receptors ($GABA_A$Rs). Importantly, TC neurons also express extrasynaptic $\alpha4\beta2\delta$ $GABA_A$Rs, although how they cooperate with synaptic $GABA_A$Rs to influence relay cell inhibition, particularly during physiologically relevant nRT output, is unknown. To address this question, we performed paired whole-cell recordings from synaptically coupled nRT and TC neurons of the ventrobasal (VB) complex in brain slices derived from wild-type and extrasynaptic $GABA_A$R-lacking, $\alpha4$ "knock-out" ($\alpha4^{0/0}$) mice. We demonstrate that the duration of VB phasic inhibition generated in response to nRT burst firing is greatly reduced in $\alpha4^{0/0}$ pairs, suggesting that action potential-dependent phasic inhibition is prolonged by recruitment of extrasynaptic $GABA_A$Rs. Furthermore, the influence of nRT tonic firing frequency on VB holding current is also greatly reduced in $\alpha4^{0/0}$ pairs, implying that the $\alpha4$-$GABA_A$R-mediated tonic conductance of relay neurons is dynamically influenced, in an activity-dependent manner, by nRT tonic firing intensity. Collectively, our data reveal that extrasynaptic $GABA_A$Rs of the somatosensory thalamus do not merely provide static tonic inhibition but can also be dynamically engaged to couple presynaptic activity to postsynaptic excitability. Moreover, these processes are highly sensitive to the δ-selective allosteric modulator, DS2 and manipulation of GABA transport systems, revealing novel opportunities for therapeutic intervention in thalamocortical network disorders.

Introduction

Thalamocortical (TC) networks support several sleep-related brain rhythms and govern many integrative processes, including attention, cognition, and sensorimotor processing (Sherman and Guillery, 2001; Steriade, 2003; Timofeev, 2011). Within this network, reciprocal intrathalamic connections between inhibitory thalamic reticular nucleus (nRT) and excitatory TC relay neurons play a critical role in controlling information transmission to cortex (Huguenard and McCormick, 2007). Abnormalities within this circuitry have also been implicated in some neurological disorders, including absence seizures and schizophrenia (Crunelli and Leresche, 2002; Pinault, 2011). In all aspects, the firing patterns of thalamic neurons are crucial. Both nRT and relay cells exhibit burst or tonic firing modes, with burst generation dependent on the activation of T-type Ca^{2+} channels (Jahnsen and Llinas, 1984; Avanzini et al., 1989; Crunelli et al., 1989). These distinct firing patterns are commonly ascribed to different conscious states: tonic firing dominates during waking, whereas burst firing prevails during periods of drowsiness and NREM sleep (Sherman and Guillery, 2001; Steriade, 2003).

The nRT plays an essential role in thalamocortical network operations, providing a major source of inhibition to relay neurons. Such inhibition is mediated predominantly by the activation of $GABA_A$ receptors ($GABA_A$Rs), with an additional contribution from $GABA_B$Rs during intense nRT output (Cox et al., 1997; Kim et al., 1997; Beenhakker and Huguenard, 2010). In the somatosensory thalamus, relay neurons exhibit two temporally and kinetically distinct modes of $GABA_A$R-mediated inhibition: brief phasic inhibition mediated by synaptic $\alpha1\beta2\gamma2$ receptors and a persistent tonic inhibition mediated by extrasynaptic $\alpha4\beta2\delta$ receptors (Belelli et al., 2005; Cope et al., 2005; Jia et al., 2005; Chandra et al., 2006; Peden et al., 2008). However, it is unknown how synaptic and extrasynaptic $GABA_A$Rs ($eGABA_A$Rs) cooperate to regulate thalamocortical output, particularly during physiologically relevant patterns of nRT activity. Given the established link between membrane potential and TC output mode, an important activity-dependent role for both tonic and phasic inhibition may be envisaged. Indeed, activation of $eGABA_A$Rs may facilitate tonic to burst firing transitions by promoting neuronal hyperpolarization (Cope et al., 2005). Furthermore, large, prolonged IPSPs generated in response to nRT

Received March 15, 2013; revised July 5, 2013; accepted Aug. 11, 2013.

Author contributions: M.B.H., J.J.L., and D.B. designed research; M.B.H. and A.R.B. performed research; M.B.H. and A.R.B. analyzed data; M.B.H., J.J.L., and D.B. wrote the paper.

This work was supported by Epilepsy Research United Kingdom Fellowship F1001 to M.B.H., a British Pharmacological Society A.J. Clark studentship to A.R.B., Tenovus Scotland (M.B.H., D.B., and J.J.L.), and the Anonymous Trust (M.B.H., D.B., and J.J.L.). We thank Dr. Thomas Rosahl (Merck Sharp and Dohme) and Prof. Gregg Homanics (University of Pittsburgh) for provision of the $\alpha1^{0/0}$ and $\alpha4^{0/0}$ mice, respectively; Dr. John Dempster (University of Strathclyde) for WinEDR software modifications required for simulations; and Dr. László Acsády (Institute of Experimental Medicine, Hungarian Academy of Sciences) and Dr. Anita Lüthi (University of Lausanne) for sharing unpublished data.

The authors declare no competing financial interests.

*J.J.L. and D.B. contributed equally to this work as senior authors.

Correspondence should be addressed to Dr. Murray B. Herd, Division of Neuroscience, Medical Research Institute, University of Dundee, Ninewells Hospital and Medical School, Dundee, DD1 9SY, United Kingdom. E-mail: m.b.herd@dundee.ac.uk.

A. R. Brown's present address: Pfizer Neusentis, Portway Building, Granta Park, Cambridge, CB21 6GS, United Kingdom.

DOI:10.1523/JNEUROSCI.1174-13.2013

 0270-6474/13/3314850-19$15.00/0

spike bursts can trigger postinhibitory rebound spike bursts in relay neurons, a phenomenon crucial to intrathalamically generated spindle oscillations (von Krosigk et al., 1993; Kim et al., 1997; Steriade, 2003; Sohal et al., 2006). However, the contribution (if any) of eGABA$_A$Rs in sculpting inhibition generated by burst and tonic nRT output modes remains unknown. Such knowledge is crucial to fully understand the role of inhibitory mechanisms in fine-tuning behaviors contingent upon the TC network.

We address this question using paired recordings from synaptically coupled nRT and relay neurons of the ventrobasal complex in wild-type (WT) and eGABA$_A$R-lacking ($\alpha4^{0/0}$) mouse brain slices. We demonstrate that α4-GABA$_A$Rs contribute to nRT burst-mediated inhibition and that activity-dependent recruitment of eGABA$_A$Rs dynamically influences the VB neuron tonic conductance during nRT tonic spike trains. Such responses are also highly sensitive to selective allosteric modulation of δ-containing eGABA$_A$Rs and manipulation of GABA transport systems, revealing novel opportunities for pharmacological intervention in disorders of the thalamocortical network.

Materials and Methods

Breeding of mice. The $\alpha1^{0/0}$, $\alpha4^{0/0}$, and $\delta^{0/0}$ mice were generated on a mixed C57BL/6J-129SvEv ($\alpha1^{0/0}$) or single C57BL6 ($\alpha4^{0/0}$ and $\delta^{0/0}$) background at the Merck Sharp and Dohme Research Laboratories at the Neuroscience Research Centre in Harlow and at the University of Pittsburgh, respectively, as described previously (Mihalek et al., 1999; Sur et al., 2001; Chandra et al., 2006). Brain slices were prepared from the first two generations of WT, $\alpha1^{0/0}$, $\alpha4^{0/0}$, and $\delta^{0/0}$ breeding pairs derived from the corresponding heterozygous mice bred at the University of Dundee.

Slice preparation. Animals were killed by cervical dislocation in accordance with Schedule 1 of the United Kingdom Government Animals (Scientific Procedures) Act 1986. Thalamic slices were prepared from mice of either sex (P15–P23) according to standard protocols (Belelli et al., 2005). Dissected brains were sliced horizontally (300–350 μm) in an ice-cold sucrose-based cutting solution, using a Vibratome (Intracel, Royston). The slices were incubated at room temperature (20–23°C) for a minimum of 1 h before recording in an oxygenated, extracellular solution (ECS) containing the following (in mM): 126 NaCl, 2.95 KCl, 26 $NaHCO_3$, 1.25 NaH_2PO_4, 2 $CaCl_2$, 10 D-glucose, and 2 $MgCl_2$ (pH 7.4; 300–310 mOsm).

Electrophysiology. Electrophysiological recordings were performed from thalamic slices maintained in warmed ECS (30°C unless otherwise stated), using one or two Axopatch 200B amplifiers (Molecular Devices), from single thalamic VB neurons (for recording electrically evoked IPSCs, or tonic currents), or from synaptically coupled presynaptic nRT neurons and postsynaptic VB neurons. Cells were visually identified with an Olympus BX51 microscope (Olympus), equipped with differential interference contrast/infrared optics and a CCD camera.

Single-cell, whole-cell recordings. Whole-cell voltage- and current-clamp recordings from VB neurons were obtained using patch pipettes prepared from thick-walled borosilicate glass (King Precision Glass), using a Narishige PC-10 vertical puller, and had open tip resistances of 4.5–6 MΩ when filled with a solution containing the following (in mM): 130 K-Gluconate, 2 KCl, 2 NaCl, 10 HEPES, 0.2 EGTA, 2 Mg-ATP, 0.5 Na-GTP, 10 Tris-phosphocreatine, osmolarity 280–290 mOsm, pH 7.2–7.3 with KOH. Inhibitory responses were evoked in VB neurons, using a bipolar tungsten electrode (World Precision Instruments), placed within the borders of the nRT. Stimuli were delivered (20 μs duration, 0.05–0.1 Hz) using a Digitimer DS3 Isolated Stimulator (Digitimer). Although we find that GABA$_B$ receptor activation is minimal under these recording conditions/stimulation parameters (data not shown), we performed the experiments in the presence of CGP 55845 (1 μM) to block GABA$_B$ receptors. Evoked IPSCs (eIPSCs) were recorded at a holding potential of −50 mV (GABA Erev ~ −85 mV). eIPSPs were recorded and quantified at V_m ~ −52 to −55 mV, with some eIPSPs also recorded at additional potentials (ranging from −80 to −40, 10 mV increments). Series resistance was intermittently monitored, compensated by up to 80% (for voltage-clamp) and recordings discarded if values changed by >25%, or increased beyond 25 MΩ. A liquid junction potential of ~14 mV was left uncorrected. Recordings were filtered at 2 or 5 kHz for voltage- and current-clamp recordings, respectively, and acquired directly to PC using a NI-DAQmx analog-digital interface (National Instruments United Kingdom) for subsequent offline analysis.

To record VB tonic currents, experiments were performed as we previously described (Belelli et al., 2005; Peden et al., 2008; Herd et al., 2009). Briefly, whole-cell recordings were obtained using patch pipettes (prepared as above) with open tip resistances of 3–5 MΩ when filled with an intracellular solution containing the following (in mM): 140 CsCl, 10 HEPES, 10 EGTA, 2 Mg-ATP, 1 $CaCl_2$, 5 QX-314, pH 7.3, with CsOH, 300–305 mOsm. Cells were recorded at a holding potential of −60 mV in ECS (as above) that additionally contained 2 mM kynurenic acid and 0.5 μM tetrodotoxin to block ionotropic glutamate receptors and sodium-dependent action potentials, respectively. The tonic current was calculated as the difference between the holding current before and after application of bicuculline methobromide.

Paired recordings. Paired whole-cell recordings were performed from synaptically coupled presynaptic nRT neurons and postsynaptic VB neurons, using patch electrodes prepared as described above. Presynaptic electrodes were filled with the same K-gluconate solution used for eIPSC/IPSP recordings, whereas in the majority of recordings, postsynaptic electrodes were filled with an intracellular solution containing the following (in mM): 105 Cs-gluconate, 30 KCl, 2 NaCl, 10 HEPES, 0.2 EGTA, 2 Mg-ATP, 0.5 Na-GTP, 10 Tris-phosphocreatine, osmolarity 280–290 mOsm, pH 7.2–7.3 with CsOH. In a subset of paired recordings, postsynaptic VB cells were patched using the same low Cl^-, K-gluconate-based ICS solution used for presynaptic electrodes. Presynaptic nRT neurons were recorded under current-clamp, whereas postsynaptic VB neurons were recorded in voltage-clamp mode (V_h = −70 mV or −50 mV, GABA$_A$R Erev ~ −40 mV or −85 mV for Cs-gluconate and K-gluconate-based solutions, respectively). The locations chosen for patching within slices were based on the topographical organization of nRT-VB connections (Lam and Sherman, 2005). In the majority of cases, successful identification of nRT-VB pairs was facilitated by first patching the VB neuron, then applying a low-pressure stream of a high-K^+ solution from a "sniffer" pipette moved within candidate regions of the nRT (Gentet and Ulrich, 2003). If the region contained one or more presynaptic partners, a burst of IPSCs was observed in the VB neuron. Up to 10 nRT neurons residing within this "hotspot" were then patched and tested for connectivity to the VB neuron. Successful pairs were characterized by the generation of a short latency (<2 ms) IPSC in the VB neuron in response to a suprathreshold stimulation of the nRT neuron. We retained only those pairs where a clear, relatively fast rising response (<1 ms 10–90% rise time) was generated by a presynaptic spike. Inhibitory postsynaptic responses were generated in response to both classical modes of action potential firing exhibited by nRT neurons (i.e., burst and tonic modes). Action potential bursts were generated within nRT neurons using a software (WinEDR) driven 30–50 ms suprathreshold current step (0.05–0.1 Hz), delivered via the recoding electrode from a sufficiently hyperpolarized V_m (usually the resting V_m). A consistent intraburst spike number (~±1 spike) was maintained throughout the recording (control and drug sections) by minimally adjusting the stimulation amplitude and/or membrane potential if necessary. Tonic trains of action potentials (APs) were elicited in nRT neurons from a depolarized V_m by injection of suprathreshold direct current. The level of injected DC was maintained at a constant amplitude for 5–10 s before being increased to enhance tonic firing frequency. Five to seven DC increments were applied during each tonic train. On termination of most paired recordings, the locations of the presynaptic and postsynaptic electrodes were observed under low-power magnification and recorded to PC using a USB video capture device connected to the output of the monitor (for a schematic illustration of the locations of a sample of successful pairs, see Fig. 3*F*,*G*). The majority of postsynaptic neurons were adjudged to be located in the ventral posteromedial nucleus (VPM).

Data analysis. All electrophysiological analyses were performed offline using the Strathclyde Electrophysiology Software, WinEDR/WinWCP (J. Dempster, University of Strathclyde, United Kingdom) software package. Action potentials generated in both burst and tonic modes were analyzed with respect to action potential number (within a burst), frequency, and interevent interval. In current-clamp recordings from VB neurons, eIPSPs were analyzed with respect to their peak, area, and time to decay from peak by 50% (T50). All postsynaptic currents (evoked, burst-, and tonic-mediated IPSCs) were analyzed with respect to peak amplitude, 10–90% rise time, and charge transfer. For tonic-mediated IPSCs (tIPSCs), a depressing synapse phenotype was defined if the peak amplitude ratio of the second tIPSC versus first tIPSC during a tonic train was <1. The decay time course of all three types of synaptic current was described adequately in the majority of cases by fitting a double exponential function ($y(t) = A_1e^{(-t/\tau 1)} + A_2e^{(-t/\tau 2)}$) using the least-squares method, where A is amplitude, t is time, and τ is the decay time constant. Analysis of the SD of residuals and use of the F test were used to compare goodness of fit, confirming an improved fit of the decay was achieved when using a double exponential rather than a monoexponential. Thus, a weighted decay time constant (τw) was also calculated according to the equation as follows:

$$\tau w = \tau_1 P_1 + \tau_2 P_2,$$

where τ_1 and τ_2 are the decay time constants of the first and second exponential functions and P_1 and P_2 are the proportions of the synaptic current decay described by each component. For multipeak events (i.e., eIPSC and burst-mediated IPSCs), only the decay phase occurring after the final peak of the event was curve-fitted. For tIPSCs, currents generated in response to the first 500 APs in the train were binned sequentially (50 events per bin minus failures), and each of the 10 event bins was then averaged. The decay of each bin average was fitted with a biexponential function as described above. A "global" average of tIPSC responses to the first 500 (nonbinned) APs was also generated and used to further compare strain and drug effects. As the experimental paradigm dictates, these early APs occur at relatively low frequencies (19 ± 1 Hz for both WT and $\alpha4^{0/0}$). Therefore, each individual tIPSC has sufficient time to fully decay to baseline before the onset of subsequent events, thus facilitating an accurate determination of tIPSC decay kinetics. The reliability of nRT-VB connections was determined by analysis of the postsynaptic current response to the first 50 nRT APs at each frequency increment. Transmission success was defined by the presence of a postsynaptic response with an amplitude >4× the SD of baseline noise (generally 3–4 pA), occurring within a 4 ms latency from the presynaptic spike.

In nRT-VB pairs, the influence of nRT tonic firing frequency on VB holding current (I_{hold}) was determined by sampling 3 ms I_{hold} sections immediately before the onset of each tIPSC throughout the course of the tonic train. Baseline VB I_{hold} values were determined by sampling 10 ms sections (6/s) for 15–20 s before and after the tonic train. The change in VB I_{hold} (relative to baseline values) was determined for each increment in nRT firing frequency (averaged over each 5–10 s increment). For summary nRT frequency-VB I_{hold} plots (e.g., see Fig. 4*G*), data were plotted in 5 Hz bins. Linear regression analysis was performed, and the slope of the resultant linear fits used to compare the influence of nRT firing frequency on VB I_{hold} in WT and $\alpha4^{0/0}$ mice.

All results are reported as the arithmetic mean ± SEM. Statistical significance of the mean data was assessed with the Student's t test (paired or unpaired), or repeated-measures ANOVA (one- or two-way) as appropriate, using the SigmaStat (SPSS) software package. Linear regression was performed in Origin v7 (OriginLab).

Simulations. To evaluate the specific contribution of tIPSC kinetics to baseline changes of the holding current observed in response to increasing presynaptic firing frequencies, we performed some simple computer simulations using the WinEDR (V3.3.8) postsynaptic current simulator. The simulations used mean values derived from the detailed analysis of *in vitro* paired recordings (see Fig. 5). Simulation parameters included the following: (1) initial IPSC amplitude ± SD, (2) IPSC rise time constant, (3) IPSC decay time constant, (4) percentage value for IPSC amplitude depression, (5) time constant of synaptic depression, (6) IPSC frequency ± SD, and (7) baseline noise. All parameters remained constant during each simulation, with the exception of IPSC frequency, which was increased in 5 Hz increments from 7.5 ± 1.5 Hz to 52.5 ± 1.5 Hz (5 s per increment), and peak amplitude, which incorporated an initial rapid depression (% depression = 56–58%; time constant of depression, τ_{dep} = 0.38 s). Changes in the baseline current over the course of each simulation were measured in the same manner as for *in vitro* tIPSC experiments (see above). The influence of IPSC kinetics on the baseline current was investigated by setting the IPSC decay time constant to match the mean tIPSC τw values derived from WT and $\alpha4^{0/0}$ recordings under control conditions, or in the presence of drugs. To assess the effect of IPSC amplitude in relation to IPSC kinetics, these simulations were repeated, except that the initial peak amplitude was set to match those of the "strongest" and "weakest" connections, rather than the mean IPSC amplitude. A total of six simulations were run for each condition.

Salts and drugs. DS2 (supplied by Dr. K. Wafford), CGP 55835 (Abcam), and SNAP 5114 (Tocris Bioscience) were prepared in DMSO as 1000-fold concentrated stock solutions and diluted in ECS to the final desired concentration. The final DMSO concentration (0.1%) has no effect on any of the measured parameters. NO-711 (Abcam) was prepared as a 1000× aqueous stock solution and diluted in ECS as required. Nipecotic acid (Abcam) was prepared in ECS at the final concentration (1 mM). All drugs were applied via the perfusion system (2–4 ml/min) and allowed to infiltrate the slice for a minimum of 10 min (with the exception of SNAP 5114, which we find requires >20 min application to reach full effect) while recordings were acquired. All other salts and drugs were obtained from Sigma, Tocris Bioscience, or VWR, with the exception of Cs-gluconate, which was prepared and provided by Dr. A. Rozov (University of Dundee).

Results

Activation of α4-GABA$_A$Rs prolongs evoked IPSCs of VB neurons

Although detailed ultrastructural studies of α4 and δ subunit distribution have yet to be performed in thalamus, immunohistochemical studies have repeatedly demonstrated that α4 or δ subunits do not colocalize with synaptic markers in thalamic relay neurons, thus inferring a predominantly extrasynaptic localization of α4/δ-GABA$_A$Rs (Jia et al., 2005, 2007; Kralic et al., 2006; Peden et al., 2008). Indeed, genetic deletion of α4 or δ subunits has previously been shown to greatly reduce the tonic inhibitory conductance recorded from VB neurons, with minimal impact on miniature IPSCs (Chandra et al., 2006; Herd et al., 2009). In agreement with Chandra et al. (2006), the VB tonic current revealed upon application of bicuculline (30 μM) was greatly reduced in $\alpha4^{0/0}$ mice compared with WT under our recording conditions (Fig. 1*A*,*B*). Importantly, deletion of the α4 subunit reduced the tonic current to values indistinguishable from those we previously described for $\delta^{0/0}$ VB neurons (Herd et al., 2009) (Fig. 1*C*,*D*). Although compensatory mechanisms may be a consequence of global gene knock-out strategies (Brickley et al., 2001), the tonic current experiments demonstrate that the remaining palette of GABA$_A$R subunits expressed by VB neurons of $\alpha4^{0/0}$ or $\delta^{0/0}$ mice do not appear to compensate for the absent extrasynaptic receptors. Therefore, both lines offer a suitable model to investigate whether eGABA$_A$Rs, in addition to their established role during tonic inhibition, may contribute to inhibitory synaptic transmission generated in response to nRT output. Thus, in preliminary experiments, we compared the properties of electrically eIPSCs recorded from VB neurons of WT, $\alpha4^{0/0}$, and $\delta^{0/0}$ mice. In all strains, brief extracellular stimulation of nRT evoked outward VB IPSCs characterized by multiple peaks and a biexponential decay (Fig. 2*A*). The, multipeak nature of individual eIPSCs is consistent with the generation of I_T-dependent spike bursts, within one or more presynaptic nRT neurons. In

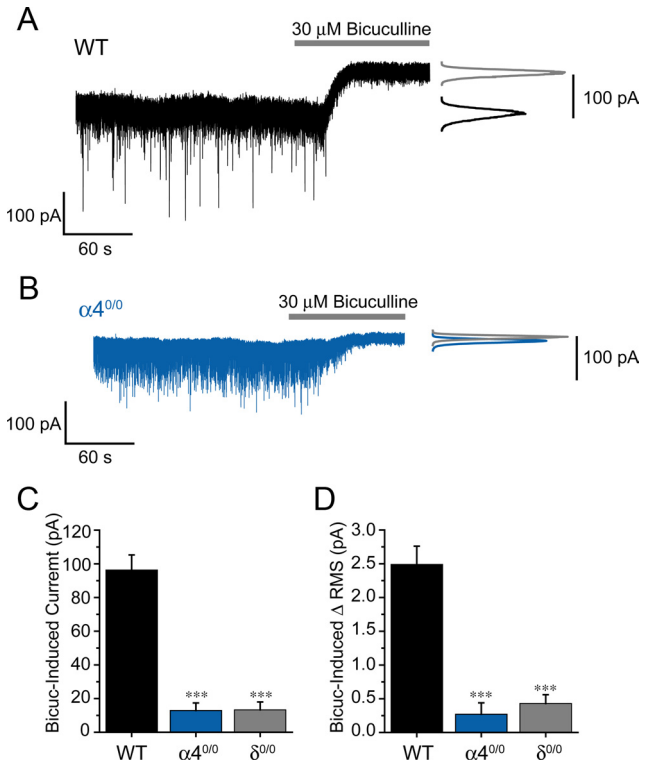

Figure 1. The tonic inhibitory conductance of VB neurons is greatly reduced by deletion of the α4 subunit. ***A***, ***B***, Representative whole-cell recordings (left) and corresponding all points histograms (right) illustrating the effect of bicuculline (30 μM, gray bars) on the holding current of VB neurones derived from WT (black) and $\alpha4^{0/0}$ (blue) mice. ***C***, ***D***, Bar graphs illustrating the outward current (***C***) and the change in RMS noise (***D***) induced by bicuculline in WT ($n = 27$, black bars) and $\alpha4^{0/0}$ ($n = 12$, blue bars) VB neurons. For comparison, values derived from $\delta^{0/0}$ VB neurons (gray bars; data from Herd et al., 2009), under identical recording conditions, are included in the bar graph. There is a lack of a significant difference for $\alpha4^{0/0}$ versus $\delta^{0/0}$ values ($p = 0.92$ and $p = 0.49$ for the bicuculline-induced change in holding current and RMS respectively, unpaired *t* test). ***$p < 0.001$ versus WT (unpaired *t* test).

recordings performed from $\alpha4^{0/0}$ and $\delta^{0/0}$ slices, eIPSCs displayed similar amplitudes to WT currents (Fig. 2*A*,*B*). However, the decay kinetics of both $\alpha4^{0/0}$ and $\delta^{0/0}$ eIPSCs were significantly faster than WT eIPSCs (Fig. 2*A*,*C*). Consequently, the charge transferred per eIPSC was significantly reduced in $\alpha4^{0/0}$ and $\delta^{0/0}$ VB neurons (Fig. 2*D*). No significant difference in eIPSC peak amplitude, τw, or charge transfer was observed between $\alpha4^{0/0}$ and $\delta^{0/0}$, confirming for both lines the loss of $\alpha4\beta\delta$ GABA$_A$Rs. Importantly, when recordings were performed at 37°C, the impact of α4 subunit deletion upon all the above parameters was preserved (peak amplitude: WT = 386 ± 41 pA, $\alpha4^{0/0}$ = 423 ± 43 pA, $p = 0.54$; τw: WT = 28 ± 4 ms, $\alpha4^{0/0}$ = 9 ± 1 ms, $p = 0.0007$; charge transfer: WT = 14 ± 2 fC, $\alpha4^{0/0}$ = 7 ± 1 fC, $p = 0.01$, unpaired *t* test; $n = 8$ and 7 for WT and $\alpha4^{0/0}$, respectively). These results suggest that the contribution of eGABA$_A$Rs to the IPSC decay time is not a consequence of the recording temperature (30°C) used routinely in this study.

Our results predict that VB neurons devoid of synaptic GABA$_A$Rs should retain an eGABA$_A$R-mediated inhibitory response to presynaptic stimulation. We previously demonstrated that deletion of the α1 subunit abolishes VB mIPSCs, with no effect on the tonic current, thereby providing a model to test this hypothesis (Peden et al., 2008). Remarkably, $\alpha1^{0/0}$ VB neurons exhibited a robust, residual eIPSC, albeit of reduced peak amplitude, but with a similar τw to WT (Fig. 2*A*–*D*). Importantly, the 10–90% rise times of $\alpha1^{0/0}$ eIPSCs were greatly increased relative

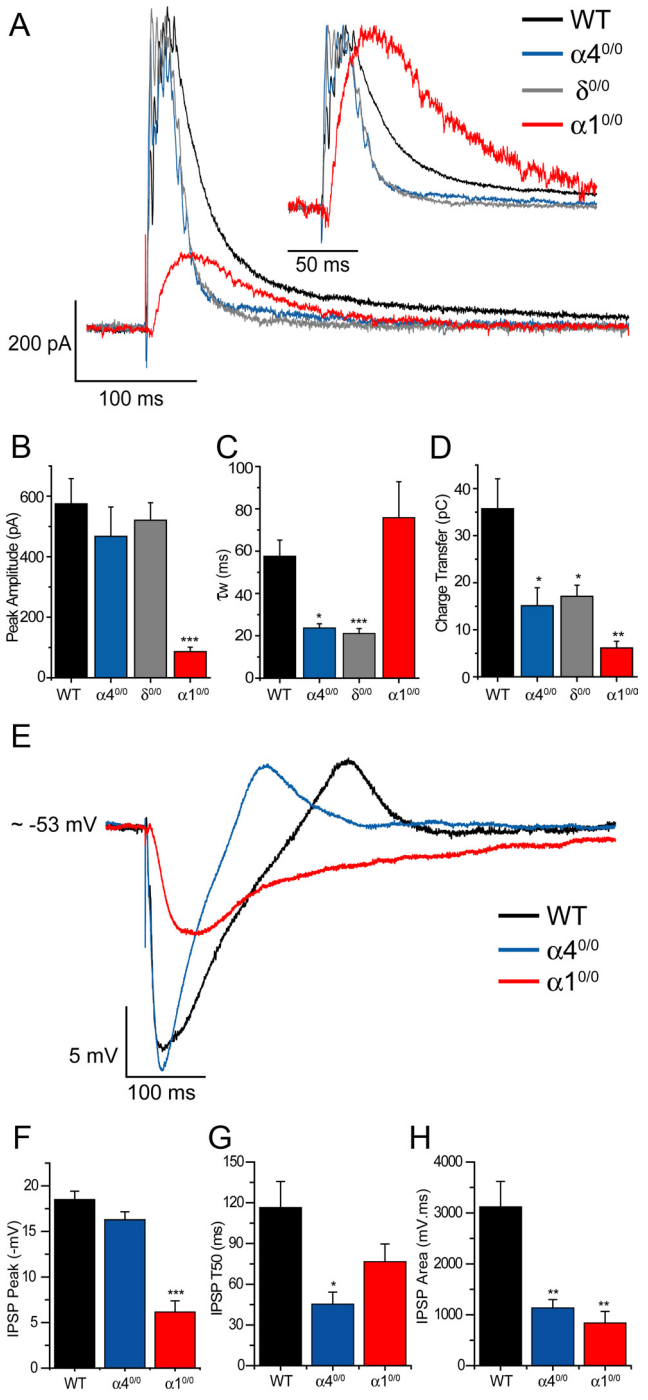

Figure 2. Activation of $\alpha4\beta\delta$-GABA$_A$Rs prolongs the duration of evoked IPSCs recorded from VB neurons. ***A***, Superimposed, representative eIPSCs recorded from WT (black), $\alpha4^{0/0}$ (blue), $\delta^{0/0}$ (gray), and $\alpha1^{0/0}$ (red) VB neurons in response to extracellular stimulation of the nRT (single stimuli, 20 μs duration, 0.1 Hz frequency). Inset, Peak-scaled traces are illustrated to facilitate comparison of the eIPSC decay phases recorded from each mouse strain. ***B–D***, Bar graphs comparing eIPSC peak amplitude (***B***), τw (***C***), and charge transfer (***D***) recorded from VB neurons derived from WT (black bars, $n = 13$), $\alpha4^{0/0}$ (blue bars, $n = 5$), $\delta^{0/0}$ (gray bars, $n = 9$), and $\alpha1^{0/0}$ mice (red bars, $n = 8$). There is a lack of a significant difference between eIPSC τw, or charge transfer for $\alpha4^{0/0}$ versus $\delta^{0/0}$ ($p = 0.46$ and $p = 0.64$ for τw and charge transfer, respectively, unpaired *t* test). ***E***, Superimposed eIPSPs recorded under current-clamp conditions from WT, $\alpha4^{0/0}$, and $\alpha1^{0/0}$ VB neurons in response to extracellular stimulation of the nRT. ***F–H***, Bar graphs comparing eIPSP peak (***F***), T50 (***G***), and area (***H***) recorded from VB neurons derived from WT, $\alpha4^{0/0}$, and $\alpha1^{0/0}$ mice. Evoked IPSPs were recorded at $V_m \sim -52$ to −55 mV. Color scheme for ***E–H*** as outlined for ***A–D***. $n = 5$–14. *$p < 0.05$ versus WT (unpaired *t* test). **$p < 0.01$ versus WT (unpaired *t* test). ***$p < 0.001$ versus WT (unpaired *t* test).

to WT currents (WT = 1.0 ± 0.1, $n = 13$; $\alpha1^{0/0}$ = 14.9 ± 1.9, $n = 8$, $p = 5.1 \times 10^{-10}$; Fig. 2*A*). Additionally, clearly defined multiple peaks were not observed within the slow rising phase of residual $\alpha1^{0/0}$ eIPSCs, in contrast to WT, $\alpha4^{0/0}$, and $\delta^{0/0}$ recordings.

For equivalent current-clamp experiments, the brief duration of $\alpha4^{0/0}$ eIPSCs was mirrored by a reduced eIPSP T50 and area relative to WT recordings (Fig. 2*E–H*). Furthermore, in $\alpha1^{0/0}$ recordings, residual eIPSPs were readily observed, with similar T50 s to WT (Fig. 2*E–H*). However, unlike most WT (10 of 14 cells) and $\alpha4^{0/0}$ (6 of 8 cells) recordings, eIPSPs recorded from $\alpha1^{0/0}$ neurons were of insufficient amplitude to generate a rebound low-threshold Ca^{2+} potential, at least at the limited range of membrane potentials studied here (Fig. 2*E*). These experiments suggest that burst-mediated GABA release in response to a single stimulus is sufficient to recruit eGABA$_A$Rs thus increasing IPSP duration.

Paired nRT-VB recordings reveal α4-GABA$_A$R activation prolongs burst-mediated IPSCs

The electrically evoked experiments described above provide preliminary evidence that α4βδ GABA$_A$Rs could play a role during phasic inhibition of VB neurons. However, such experiments do not permit exact control over the number of presynaptic cells and/or axons activated. Thus, it is conceivable that a near synchronous release of GABA from multiple axons in response to electrical stimulation could overwhelm GABA transport capacity, leading to transmitter accumulation. By contrast, paired, whole-cell recordings of monosynaptically coupled nRT and VB neurons allow the nRT action potential discharge pattern (i.e., burst, or tonic firing) to be regulated more precisely, thus providing a more refined insight into the activity-dependent properties of inhibition at monosynaptic connections. Using this approach, we compared the properties of WT and $\alpha4^{0/0}$ VB IPSCs generated in response to presynaptic nRT spike bursts (bIPSCs).

Although connections varied in strength (peak amplitude range = −46 to −463 pA; mean peak amplitude = −142.3 ± 20.0 pA; coefficient of variation (CV) = 0.73, $n = 27$ pairs), nRT bursts in successful pairs (mean spikes/burst = 7.0 ± 0.3; average frequency = 233.3 ± 7.4 Hz; for stimulation details, see Materials and Methods) generated reliable, multipeak VB bIPSCs, with each presynaptic spike generally evoking a corresponding peak within the bIPSC (Fig. 3*A*, bottom inset). In $\alpha4^{0/0}$ pairs, equivalent stimulation of nRT neurons generated similar AP bursts (mean spikes/burst = 6.1 ± 0.3; average frequency = 206.2 ± 11.2 Hz), together with corresponding multipeak bIPSCs in postsynaptic VB neurons (Fig. 3*B*, $n = 22$ pairs). The amplitude of $\alpha4^{0/0}$ bIPSCs was not significantly different from WT (Fig. 3*C*; peak amplitude range = −63.0 to −237.9 pA; mean peak amplitude = −128.6 ± 12.1 pA, $p = 0.58$ vs WT; CV = 0.44, $n = 22$). However, comparison of the synaptic current decay (see Materials and Methods) revealed that $\alpha4^{0/0}$ bIPSCs displayed a τw <50% of WT (Fig. 3*B,D*), with reduced variability (CV of τw, WT = 0.54; $\alpha4^{0/0}$ = 0.28, Fig. 3*D*) and charge transferred *per* bIPSC (Fig. 3*E*).

It has recently been reported that intracellular Cl^- concentrations directly influence the decay time of IPSCs, with physiological Cl^- levels conferring faster decay kinetics than those typically used to study GABA$_A$R function ($[Cl^-]_i > 30$ mM) (Houston et al., 2009). Therefore, to investigate whether the kinetic differences of bIPSCs observed between WT and $\alpha4^{0/0}$ are preserved using more "physiological" intracellular solutions, we repeated the paired recordings using K^+-gluconate-based pipette solutions ($[Cl^-]$ = 4 mM, GABA$_A$R Erev ~ −85 mV). In agreement with the results obtained using Cs^+-gluconate solutions ($[Cl^-]$ = 32 mM), the decay times of outward bIPSCs recorded at V_h = −50 mV were significantly reduced by deletion of the α4 subunit (WT τw = 29.0 ± 3.0 ms, $n = 9$ pairs; $\alpha4^{0/0}$ τw = 11.7 ± 1.2 ms, $n = 10$ pairs; $p = 0.00004$, unpaired t test), with no significant effect on bIPSC peak amplitude (WT = 142.6 ± 22.1 pA; $\alpha4^{0/0}$ = 176.8 ± 36.0 pA; $p = 0.44$). The presynaptic nRT spike bursts were equivalent between WT and $\alpha4^{0/0}$ pairs (spikes/burst: WT = 7.6 ± 0.3, $\alpha4^{0/0}$ = 8.2 ± 0.6, $p = 0.38$; average spike frequency: WT = 219.3 ± 14.5 Hz, $\alpha4^{0/0}$ = 244.5 ± 16.3 Hz, $p = 0.27$). Thus, the influence of α4 subunit deletion on bIPSC decay kinetics is preserved when tested using a "physiological" transmembrane Cl^- gradient. A parsimonious explanation for our results is that extrasynaptic α4βδ GABA$_A$Rs are activated during a physiologically relevant pattern of synaptic GABA release, thus increasing the duration of burst-mediated synaptic inhibition (see also below).

nRT tonic firing frequency influences VB holding current in an α4 subunit-dependent manner

Having established that eGABA$_A$Rs may be activated during intermittent burst firing, we investigated whether these receptors are similarly engaged in response to a more sustained, but far less intense, tonic discharge pattern. Utilizing paired nRT-VB recordings, we analyzed the holding current and IPSC properties of VB neurons during tonic nRT spike trains of increasing frequency. Injection of increasing direct current via the presynaptic recording electrode (Fig. 4*A*, 5–7 increments, 5–10 s duration per increment) progressively depolarized nRT neurons above AP threshold, resulting in a tonic train of spikes of increasing frequency (Fig. 4*A,B*). Such tonic trains of nRT APs evoked a stream of IPSCs (tIPSCs) in coupled VB neurons, with each AP within the train usually evoking a clear tIPSC (see below for details of IPSC success rates). In addition, a direct, albeit modest, relationship between presynaptic firing frequency and postsynaptic holding current was observed in WT (Fig. 4*A–C,G*). Although low nRT tonic firing frequencies (<15 Hz) exerted little or no influence on VB I_{hold}, increased AP discharge frequency (generally >20–25 Hz) induced an inward shift in the baseline, with subsequent increases in presynaptic AP frequency producing further inward shifts in postsynaptic I_{hold} (Fig. 4*C*). Such a relationship was particularly evident upon cessation of the nRT tonic train, whereupon a clear outward shift in VB I_{hold} was observed (Fig. 4*C*).

It is conceivable that α4βδ receptors may be progressively recruited in response to accumulation of GABA at perisynaptic/extrasynaptic domains during the course of the tonic train, thus facilitating the inward shift in VB I_{hold} observed in response to increasing nRT output frequency. To investigate this hypothesis, we repeated these experiments in neurons derived from $\alpha4^{0/0}$ mice. Importantly, the correlation between presynaptic firing frequency and postsynaptic I_{hold} was influenced by the absence of α4-containing receptors (Fig. 4*D,E*). A small, but consistent, inward shift in VB I_{hold} was observed in response to higher nRT firing frequencies (generally >25–30 Hz; Fig. 4*F*), but the effect was reduced relative to that determined for WT pairs at comparable firing frequencies (Fig. 4*G*; compare Fig. 4*C* with Fig. 4*F*). Indeed, for nRT frequency-VB I_{hold} plots (5 Hz bins, Fig. 4*G*), the linear regression fit to WT data was 2.6-fold steeper than the $\alpha4^{0/0}$ regression fit. Importantly, the difference in the slope of linear fits to frequency-I_{hold} plots obtained from WT and $\alpha4^{0/0}$ slices was preserved (3.2-fold steeper in WT) when paired record-

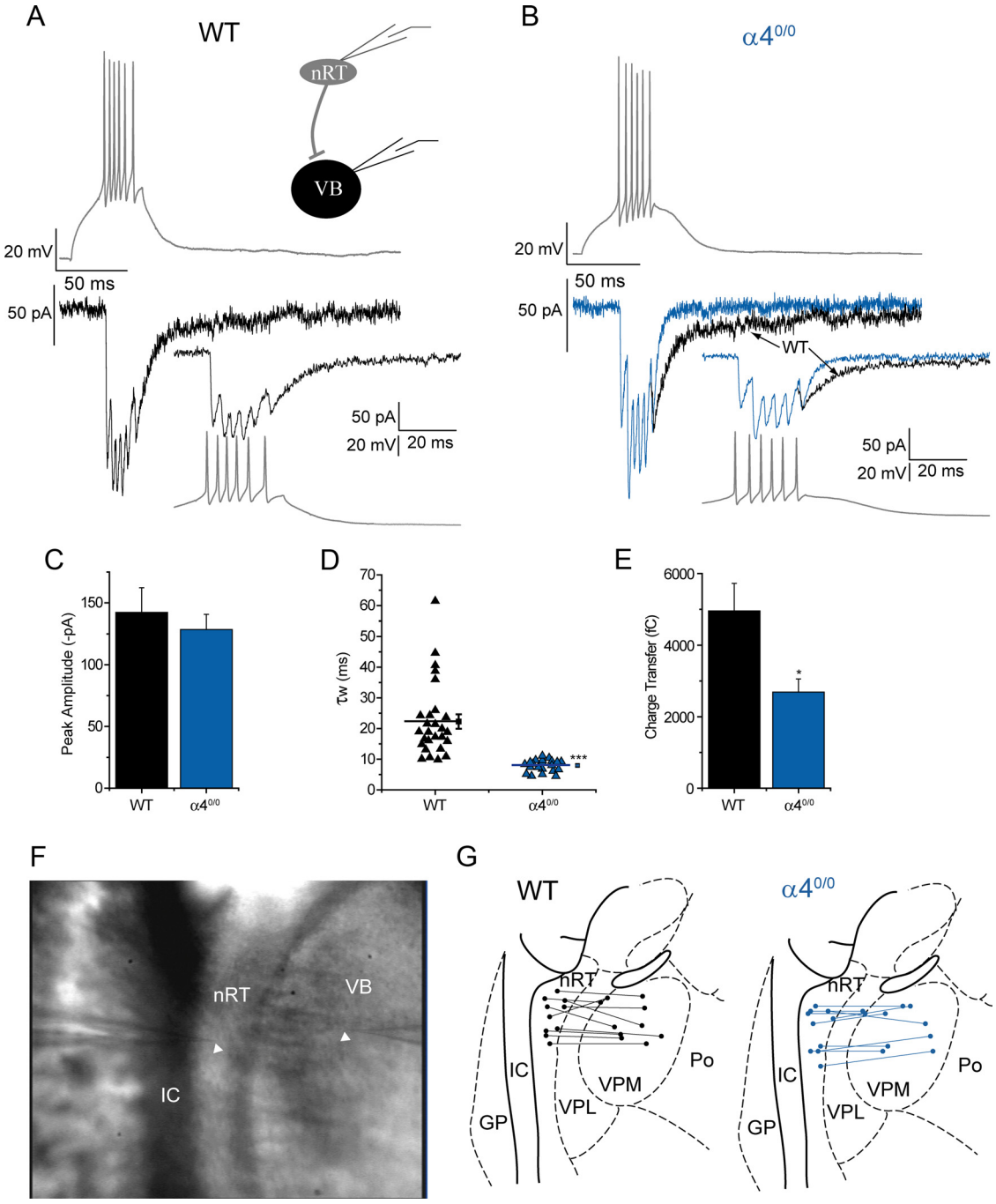

Figure 3. Deletion of the α4 subunit reduces the duration of burst-mediated IPSCs recorded from nRT-VB pairs. ***A***, Representative paired whole-cell recordings obtained from synaptically coupled WT nRT and VB neurons, illustrating a VB bIPSC (black trace, bottom) generated in response to a presynaptic nRT spike burst (gray trace, top). Top inset, Recording configuration. The same traces are illustrated on an expanded time scale in the bottom inset, with the nRT trace now lowermost to illustrate the latency from presynaptic spike to postsynaptic response. ***B***, Representative paired nRT-VB recording obtained from an $\alpha4^{0/0}$ brain slice. The panel organization is as described for ***A***, except that the $\alpha4^{0/0}$ VB bIPSC trace is blue. The decay phase of the WT bIPSC trace (black) illustrated in ***A*** has been superimposed on the decaying component of the $\alpha4^{0/0}$ bIPSC trace to emphasize the faster decay time observed in the $\alpha4^{0/0}$ neurons. ***C***, ***E***, Summary bar graphs illustrating the peak amplitude and charge transfer of bIPSCs recorded from WT (black bars, $n = 27$) and $\alpha4^{0/0}$ (blue bars, $n = 22$) nRT-VB pairs. ***D***, Scatter plot of the bIPSC τw obtained from each WT (black triangles) and $\alpha4^{0/0}$ (blue triangles) pair, illustrating the greatly reduced variability of the bIPSC decay time course in the mutant mice compared with WT. The horizontal lines, together with the filled squares to the right of each grouping, represent the mean ± SEM. $^*p < 0.05$ versus WT (unpaired *t* test). $^{***}p < 0.001$ versus WT (unpaired *t* test). ***F***, Still image obtained at low magnification of a horizontal thalamic slice and approximate recording electrode locations used for paired recordings. ***G***, Schematic illustration of a sample of 10 paired recordings obtained from WT (left) and $\alpha4^{0/0}$ (right) mice. Electrode locations are indicated by dots and synaptically coupled neurons joined by a solid line. For simplicity of illustration, the pairs are depicted on the same horizontal slice (modified with permission from Paxinos and Franklin, 2013). GP, Globus pallidus; IC, internal capsule; VPL, ventral posterolateral nucleus; VPM, ventral posteromedial nucleus (VPL + VPM = VB, ventrobasal complex); Po, posterior thalamic nucleus.

ings were performed using low "physiological" Cl^- concentrations in postsynaptic recording electrodes (Fig. 4*H*).

We next compared the properties of WT and $\alpha4^{0/0}$ tIPSCs to investigate whether any differences in IPSC parameters could contribute to the observed difference in frequency-I_{hold} relationships (Fig. 5). In agreement with previous studies demonstrating high transmission reliability in the thalamic feedback loop (Gentet and Ulrich, 2003; Evrard and Ropert, 2009), synaptic trans-

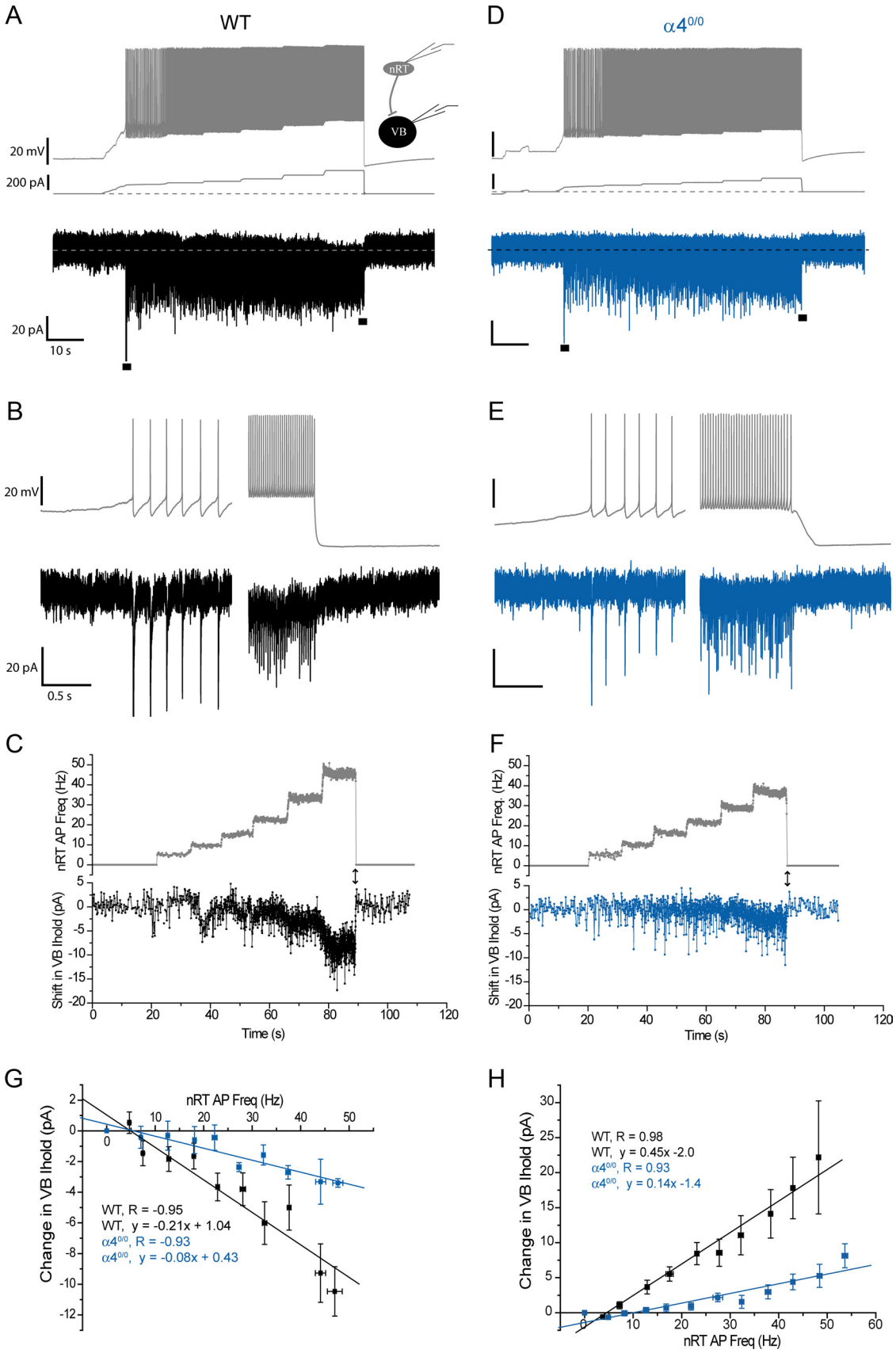

Figure 4. VB holding current is influenced by nRT tonic firing frequency. ***A***, Representative WT nRT-VB paired recording illustrating a tonic train of nRT APs occurring at increasing frequencies (top, gray) in response to incremental DC (middle, gray). The postsynaptic response (tIPSCs and baseline shift) to the tonic spike train is depicted at the bottom (black). Top inset, The recording configuration. Sections marked by horizontal black bars are expanded in ***B***. ***A***, ***B***, The first tIPSC has been truncated. ***C***, Time course plot of nRT AP frequency (top, gray) and the shift in VB I_{hold} relative to the pretrain baseline (bottom, black) for the pair illustrated in ***A***. See Materials and Methods for details of plot construction. Arrow indicates cessation of nRT spike train. (*Figure legend continues.*)

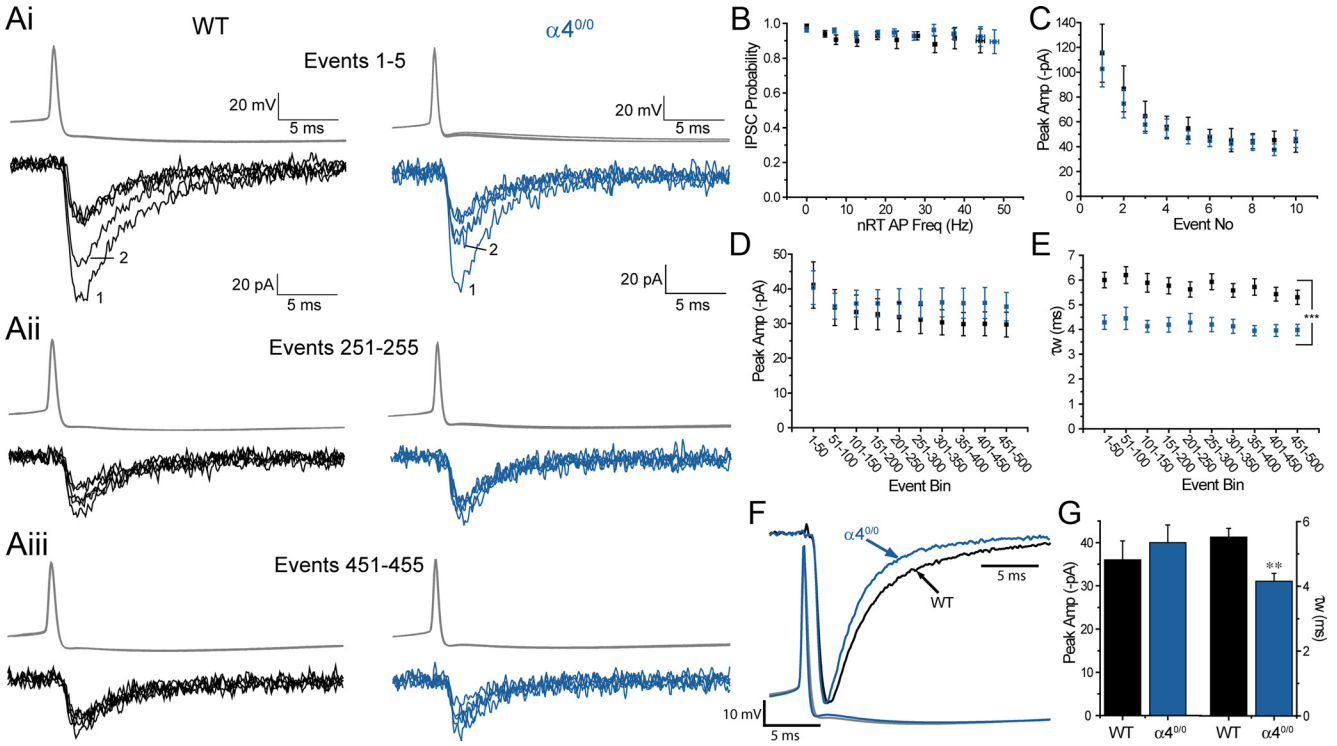

Figure 5. Deletion of the α4 subunit reduces the duration VB IPSCs generated by nRT tonic firing. ***Ai–Aiii***, Paired nRT-VB recordings obtained from WT (left) and α4 $^{0/0}$ (right) slices illustrating superimposed tIPSCs (lower traces, black represents WT; blue represents α4 $^{0/0}$) generated in response to APs 1–5 (***Ai***), 251–255 (***Aii***), and 451–455 (***Aiii***) during a tonic spike train. The tIPSCs generated by the first 2 nRT spikes are indicated in ***Ai*** to highlight the amplitude decline. ***Ai***, Scale bars are applicable to ***Aii*** and ***Aiii***. ***B***, A plot illustrating the probability of recording a tIPSC in response to nRT APs occurring at increasing frequencies (5 Hz bins) during a spike train in WT (black squares) and α4 $^{0/0}$ (blue squares) recordings. Symbols and the color scheme are also applicable to ***C–E***. ***C***, A plot of peak amplitude over the first 10 tIPSCs, illustrating a clear synaptic depression in both WT and α4 $^{0/0}$ pairs (***D***,***E***). A plot of the tIPSC peak amplitude (***D***) and τw (***E***), over the course of the first 500 events in the train. The tIPSCs were sequentially binned (50 events per bin minus failures), averaged and analyzed accordingly. There is a significant effect of the α4 subunit deletion on τw ($p = 0.0001$, two-way repeated-measures ANOVA), but no effect on peak amplitude ($p = 0.53$, two-way repeated-measures ANOVA). ***F***, Superimposed peak-scaled average tIPSCs and presynaptic APs obtained from the first 500 events (minus failures) in the WT (black represents VB; gray represents nRT) and α4 $^{0/0}$ (blue represents VB and nRT) pairs illustrated in ***A***. ***G***, A bar graph comparing the peak amplitude and τw (obtained from the "global" average of the first 500 tIPSCs) recorded from WT (black) and α4 $^{0/0}$ (blue) mice. $^{**}p < 0.01$ (unpaired *t* test).

mission at the nRT-VB synapse was highly reliable, with no failures evident in response to the first spike in the train in any WT or α4 $^{0/0}$ pair ($n = 24$ and $n = 20$, respectively). Although occasional transmission failures were evident on subsequent spikes, a strong success reliability was preserved throughout the train at each frequency increment (5 Hz bins) in the majority of recordings from both strains (IPSC probability, WT: ≥0.9 in 13 pairs and ≥0.8 in a further 5 pairs; α4 $^{0/0}$: ≥0.9 in 13 pairs and ≥0.8 in a further 4 pairs; Fig. 5*B*). However, in common with previous demonstrations of short-term depression at the nRT-VB synapse (Ulrich and Huguenard, 1996; Bessaïh et al., 2006; Evrard and Ropert, 2009), a clear and rapid depression of tIPSC amplitude was observed after the first event in the train (Fig. 5*Ai*,*C*). Although a detailed paired-pulse protocol was not performed, an exponential fit to plots of tIPSC amplitude as a function of time during the initial 50 events in the train (interspike interval = 129 ± 8 ms) revealed a time constant for synaptic depression (τ_{dep}) of 380 ± 60 ms (peak amplitude ratio of first: second tIPSC = 1: 0.79 ± 0.07 at event interval = 216 ± 28 ms). However, deletion of the α4 subunit had no effect on these properties (τ_{dep} = 400 ± 70 ms, interspike interval = 127 ± 6 ms during the first 50 APs, $p = 0.37$ vs WT; peak amplitude ratio of first: second tIPSC = 1: 0.75 ± 0.03 at event interval = 232 ± 42 ms, $p = 0.54$ vs WT, Fig. 5*C*). Indeed, there was no significant effect of genotype on tIPSC amplitude when analysis was limited to the first 10 events (when depression was close to maximal; Fig. 5*C*, $p = 0.68$, two-way repeated-measures ANOVA), or when the first 500 events (minus failures) were sequentially binned (50 events per bin) and averaged (Fig. 5*D*, $p = 0.53$, two-way repeated-measures ANOVA). By contrast, deletion of the α4 subunit significantly reduced the decay time of tIPSCs, an effect that was observed at all analyzed points within the train. For example, the decay time of the first tIPSC (effectively an isolated unitary IPSC) recorded from α4 $^{0/0}$ mice was significantly less than for equivalent WT pairs (WT τw = 6.8 ± 0.5 ms; α4 $^{0/0}$ τw = 4.5 ± 0.3 ms, $p = 0.0006$, unpaired *t* test). Similarly, we observed a significant effect of genotype when comparing the decay of sequentially averaged tIPSCs (50 events per bin, minus failures) over the course of the first 500 events in the train (Fig. 5*E*, genotype effect: $p = 0.0001$, two-way repeated-measures ANOVA; no significant genotype by event bin interaction, $p = 0.69$, two-way repeated-measures ANOVA). Thus, the decay time of "globally"

←

(*Figure legend continued.*) ***D–F***, Representative paired recording from an α4 $^{0/0}$ slice illustrating a reduced effect of presynaptic tonic firing on VB I_{hold} compared with WT. Figure details are as described for WT in ***A–C***, except that α4 $^{0/0}$ VB traces are blue. Horizontal dashed lines indicate pretonic train baseline. ***G***, Frequency-I_{hold} plot summarizing the relationship between nRT AP frequency and VB I_{hold} in WT (black, $n = 23$) and α4 $^{0/0}$ (blue, $n = 19$) pairs. Data are plotted in 5 Hz bins, and each point derived from 3 to 20 pairs. A linear regression is fitted to each dataset, and the corresponding linear equation and correlation coefficient are stated on the graph. ***H***, Same as for ***G***, except that postsynaptic electrodes contained K^+-gluconate and a lower $[Cl^-]_i$ (4 mM). Therefore, the direction of current flow is reversed and frequency-I_{hold} shifts are outward when VB cells were clamped at −50 mV. The data were derived from 6 WT and 7 α4 $^{0/0}$ recordings.

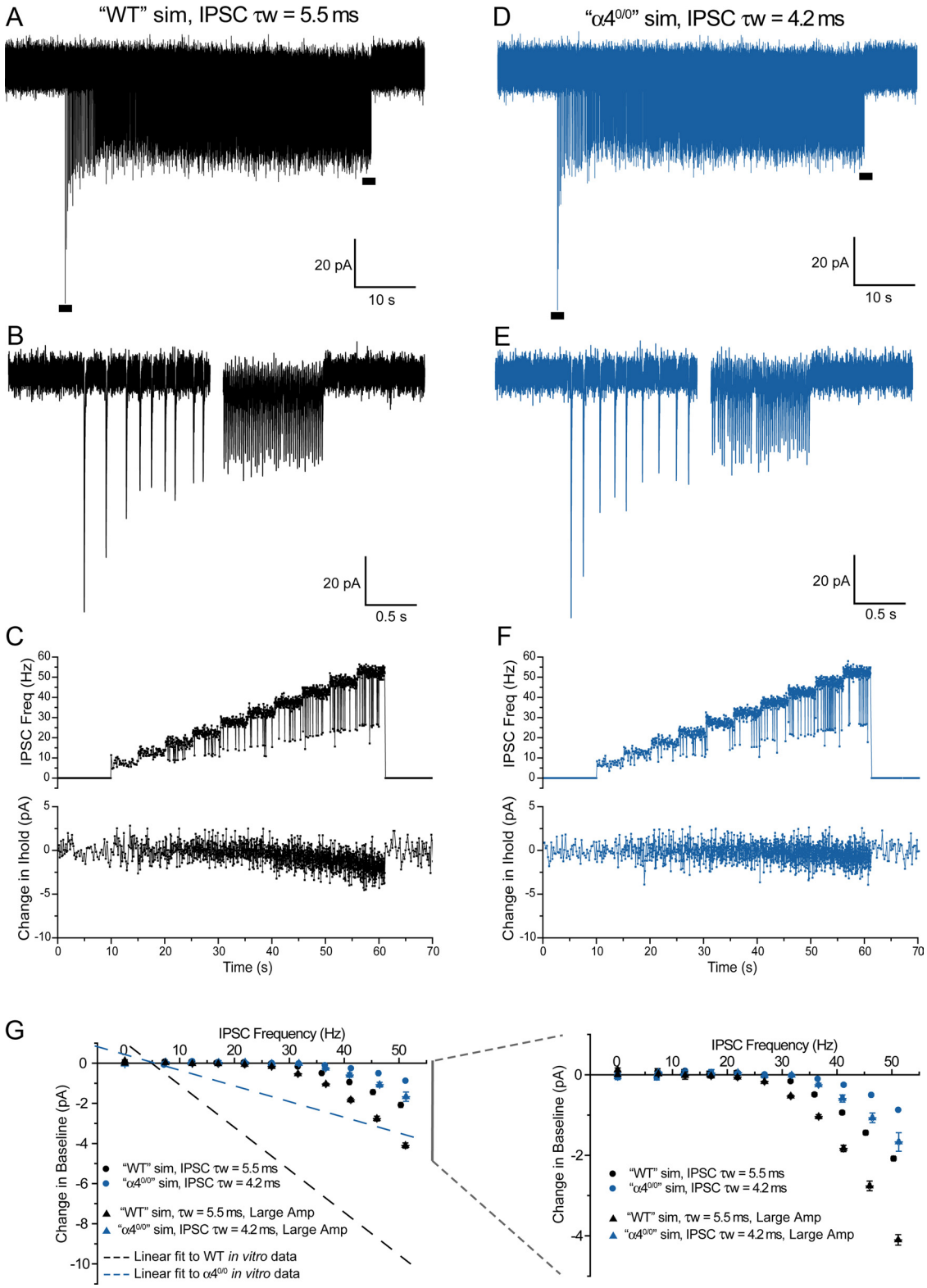

Figure 6. Summation of IPSCs during a simulated tonic train does not fully account for the nRT frequency-VB I_{hold} correlation observed *in vitro*. ***A***, ***D***, A computer simulation of a tonic train of IPSCs, with "WT" ($\tau w = 5.5$ ms, ***A***) or "$\alpha 4^{0/0}$" ($\tau w = 4.2$ ms, ***D***) kinetics occurring at increasing frequency over the course of the train (7.5–52.5 Hz, 5 Hz increments, 5 s per increment; for precise simulation details, see Materials and Methods). Two second sections indicated by the horizontal black bars are expanded below (***B***,***E***). ***C***, ***F***, A time course plot of IPSC frequency (top) and the change in the control holding current relative to the pretrain baseline (bottom) for the simulations in ***A*** and ***D***, respectively. Transient reductions in IPSC frequency observed in the top of ***C*** and ***F*** are a consequence of IPSC failures (occurring randomly at a rate of 5%). ***G***, IPSC frequency-I_{hold} plots summarizing the relationship between IPSC frequency and the resultant shift in holding current/baseline. Filled circles and filled triangles (black represents "WT"; blue represents "$\alpha 4^{0/0}$" IPSC kinetics) represent simulations using mean and large peak amplitudes respectively (values derived from *in vitro* data). The dashed lines indicate linear fits to the *in vitro* paired recordings obtained from WT (black) and $\alpha 4^{0/0}$ (blue) slices. Neither mean amplitude nor large amplitude simulations recapitulate the *in* vitro data, suggesting that IPSC summation does not predominantly account for the correlation between nRT output frequency and VB I_{hold}. The simulations are plotted on an expanded *y*-axis scale on the right.

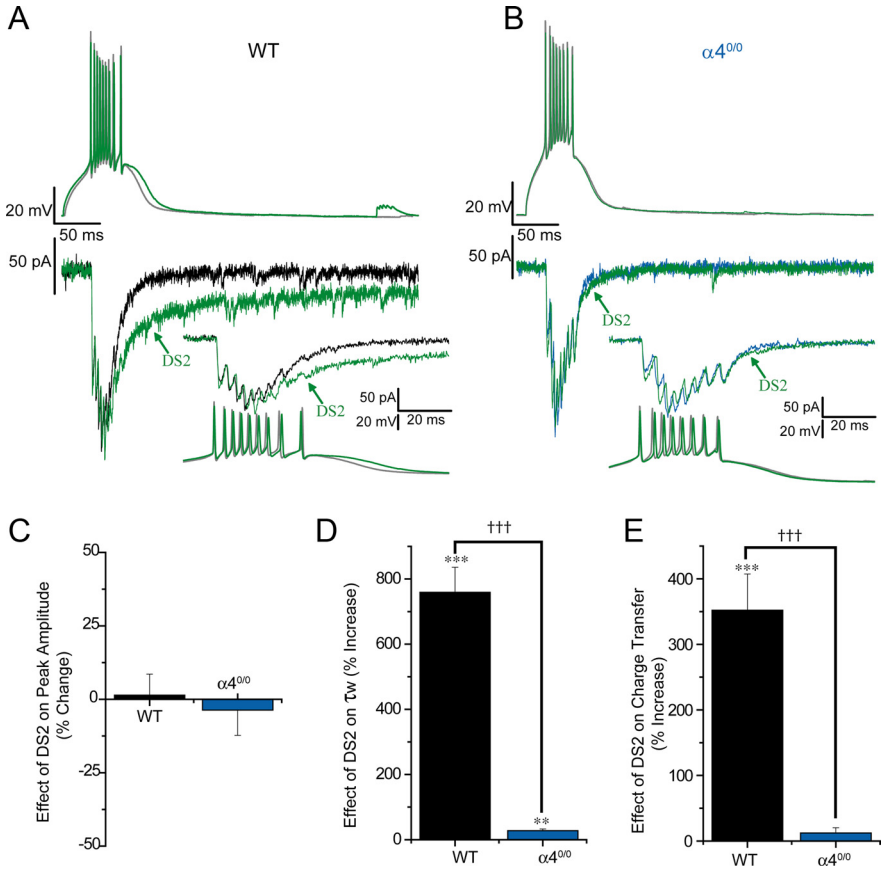

Figure 7. DS2 greatly prolongs the duration of WT, but not $\alpha4^{0/0}$ bIPSCs, in nRT-VB paired recordings. ***A***, ***B***, Representative paired nRT-VB recordings obtained from WT (***A***) and $\alpha4^{0/0}$ (***B***) mice before and after application of 10 μM DS2. Bottom, bIPSCs (black for WT control, blue for $\alpha4^{0/0}$ control, green for DS2) generated in response to presynaptic nRT spike bursts (top traces, gray represents control; green represents DS2). ***A***, ***B***, The same traces are illustrated on an expanded time scale in the bottom inset, with the nRT trace now lowermost. ***C–E***, Bar graphs illustrating the effect of DS2 on bIPSC peak amplitude (***C***), τw (***D***), and charge transfer (***E***) in WT (black bars, $n = 7$) and $\alpha4^{0/0}$ (blue bars, $n = 7$) paired recordings. $^{**}p < 0.01$ versus control (one-way repeated-measures ANOVA). $^{***}p < 0.001$ versus control (one-way repeated-measures ANOVA). †††$p < 0.001$ versus WT (two-way repeated-measures ANOVA).

averaged tIPSCs was significantly reduced for $\alpha4^{0/0}$ mice (Fig. 5*F*,*G*). Thus, α4-GABA$_A$Rs can also be recruited to shape the time course of tonic AP-dependent IPSCs in VB neurons.

These results present a scenario in which the prolonged decay time of WT tIPSCs may favor IPSC summation at higher nRT output frequencies, thus offering an alternative interpretation for the observed frequency-dependent inward shift in VB I_{hold}. To investigate this possibility, we performed a basic computer simulation comparing the effect of "WT-like" and "$\alpha4^{0/0}$-like" tIPSC kinetics on IPSC frequency-dependent baseline shifts (see Materials and Methods). The IPSC properties used during initial simulations (rise time, initial peak amplitude, τw, together with realistic values for synaptic depression) were drawn from mean values obtained from the paired recordings described above. To mimic the incremental increase in nRT AP frequency during paired recordings, IPSC frequency was increased during the simulation from 7.5 to 52.5 Hz (SD = 1.5 Hz) in 5 Hz increments (5 s per increment), and included a 5% failure rate. Figure 6*A–F* illustrates representative examples of "WT-like" and "$\alpha4^{0/0}$-like" simulations, which differ only in their IPSC decay time constants (i.e., WT IPSC τw = 5.5 ms; Fig. 6*A–C*; $\alpha4^{0/0}$ IPSC, τw = 4.2 ms, Fig. 6*D–F*). When analyzed in the same manner as *in vitro* recordings, we observed small, frequency-dependent inward shifts in the baseline of both "WT" and "$\alpha4^{0/0}$" simulations at IPSC frequencies ~>35 Hz for "WT" (Fig. 6*C*,*G*) and ~45 Hz for "$\alpha4^{0/0}$" simulations, consistent with IPSC summation. However, although the magnitude of the frequency-dependent shift was greater for tests using WT-like IPSC decay kinetics than for those using $\alpha4^{0/0}$-like properties (Fig. 6*G*, right), such simulations were clearly unable to recapitulate the *in vitro* frequency-I_{hold} relationships (Fig. 6*G*, left, dashed lines, which represent linear fits to data generated from paired recordings). Moreover, although increasing IPSC amplitude values to match those of the strongest nRT-VB connections appeared to modestly promote the frequency-dependent inward shift (Fig. 6*G*, right), such simulations still did not accurately reflect the *in vitro* data (Fig. 6*G*, left). Thus, considering these simulations, we propose that a gradual accumulation of GABA at perisynaptic/extrasynaptic domains during the tonic train enhances the activation eGABA$_A$Rs, thereby promoting VB tonic inhibition, although IPSC summation may modestly contribute to the correlation at higher firing frequencies. Regardless of the mechanism, our data reveal that the VB tonic current may be dynamically regulated by the activity of nRT neurons.

DS2, a selective δ-GABA$_A$R modulator, greatly amplifies postsynaptic inhibition induced by burst, or tonic firing

An alternative interpretation of the influence of the α4 subunit deletion on IPSC kinetics is that the observed changes arise as a consequence of the removal of synaptic α4βxγ2 rather than extrasynaptic α4βδ receptors (Sur et al., 1999). Indeed, immunogold studies suggest a limited expression the α4 subunit within synaptic regions of dentate granule cells (Sun et al., 2007; Zhang et al., 2007). However, in the thalamus, both functional studies demonstrating inhibitory actions for Ro154513 (a partial benzodiazepine "agonist" with positive allosteric activity at α4βxγ2 receptors and negative modulatory activity at equivalent receptors incorporating α1–3 or α5 subunits) (Wafford et al., 1996) and immunohistochemical evidence highlighting an apparent lack of colocalization between α4-containing receptors and synaptic markers (Jia et al., 2005, 2007; Kralic et al., 2006; Peden et al., 2008) argue against such an interpretation.

To conclusively demonstrate the specific involvement of α4βδ receptor isoforms in the thalamic functional phenotype of $\alpha4^{0/0}$, we investigated the actions of DS2 in nRT-VB paired recordings. We have shown that DS2 selectively potentiates GABA-dependent activation of δ-GABA$_A$Rs (Wafford et al., 2009; Jensen et al., 2013); and crucially, the ability of DS2 to enhance VB tonic inhibition is abolished by deletion of the δ (Jensen et al., 2013) or the α4 subunit (A.R.B., D.B., J.J.L., unpublished data). Additionally, because it is a positive allosteric modulator (cf. THIP, a preferential δ-GABA$_A$R agonist) (Belelli et al., 2005; Cope et al., 2005; Jia et al., 2005; Chandra et al., 2006; Stórustovu and Ebert,

2006; Herd et al., 2009), DS2 is an ideal pharmacological tool to probe the activation of $\alpha4\beta\delta$ GABA$_A$Rs by endogenous GABA. Given the proposed role of $\alpha4\beta\delta$ GABA$_A$Rs during AP-dependent inhibition, we hypothesized that the duration of bIPSCs and tIPSCs would be prolonged by DS2. Indeed, in WT pairs, DS2 (10 μM) dramatically increased the decay time and charge transfer of bIPSCs generated in response to comparable nRT spike bursts, with no effect on peak amplitude (Fig. 7*A*,*C–E*). Deletion of the $\alpha4$ subunit virtually abolished the effect of DS2 on bIPSC decay time and charge transfer (Fig. 7*B*,*D*,*E*), further emphasizing that deletion of $\alpha4$ effectively prevents expression of δ-containing extrasynaptic receptors.

We additionally confirmed that DS2 was similarly effective on VB neuron inhibition generated in response to extracellular stimulation of the nRT. Thus, DS2 (10 μM) greatly prolonged VB eIPSCs (τw: control = 53 ± 7 ms, DS2 = 209 ± 43 ms, $p = 0.003$, paired *t* test, $n = 7$; Fig. 8*A*) and eIPSPs, producing a delay in the timing of postinhibitory rebound low threshold Ca^{2+} potentials in cells demonstrating this property (T50: control = 178 ± 58 ms, DS2 = 473 ± 103 ms, $p = 0.05$, paired *t* test, $n = 4$; Fig. 8*B*). Moreover, in $\alpha1^{0/0}$ slices (which lack synaptic GABA$_A$Rs), DS2 significantly prolonged residual eIPSCs (τw: control = 88 ± 26 ms, DS2 = 308 ± 24 ms, $p = 0.001$, paired *t* test, $n = 5$; Fig. 8*C*) and eIPSPs (T50: control = 88 ± 16 ms, DS2 = 206 ± 45 ms, $p = 0.046$, paired *t* test, $n = 5$; Fig. 8*D*). Importantly, DS2 also increased the peak amplitude of $\alpha1^{0/0}$ eIPSCs (control = 74 ± 20 pA, DS2 = 159 ± 24 pA, $p = 0.005$) and eIPSPs (control = 5.6 ± 1.7 mV, DS2 = 8.9 ± 1.1 mV, $p = 0.02$). Collectively, these experiments provide further support for the role of $\alpha4\beta\delta$-GABA$_A$Rs in influencing the duration of inhibitory synaptic transmission during nRT burst firing.

Similarly, DS2 greatly facilitated the postsynaptic consequences of tonic firing. DS2 enhanced the frequency-I_{hold} relationship of WT nRT-VB pairs, such that the onset of an increase in nRT AP frequency produced an obvious inward "step" of the VB holding current (Fig. 9*A*,*B*). Indeed, incremental nRT output frequencies imposed a descending "staircase" shift of VB I_{hold} in the presence of DS2. Thus, in the frequency-I_{hold} plot (Fig. 9*C*), DS2 increased the slope of the linear regression fit (5.3-fold increase, $n = 6$ pairs). Additionally, DS2 significantly prolonged the tIPSC decay (Fig. 9*D*,*I*), thus supporting the conclusion that $\alpha4\beta\delta$ GABA$_A$Rs shape the properties of AP-dependent thalamic inhibition. However, incorporation of the DS2 effect on tIPSC decay into simulations as outlined above (28% increase of the mean WT control τw value) suggested that promotion of IPSC summation does not account for dramatic effect of DS2 on the frequency-I_{hold} relationship (Fig. 9*C*). In $\alpha4^{0/0}$ pairs in the presence of DS2, both the "staircase-like" frequency-I_{hold} relationship and the prolongation of tIPSCs was abolished (Fig. 9*E–I*). Thus, VB tonic current can be amplified in an activity-dependent fashion by the recruitment of additional $\alpha4$-GABA$_A$Rs, in a manner that is sensitive to modification by eGABA$_A$R-selective ligands.

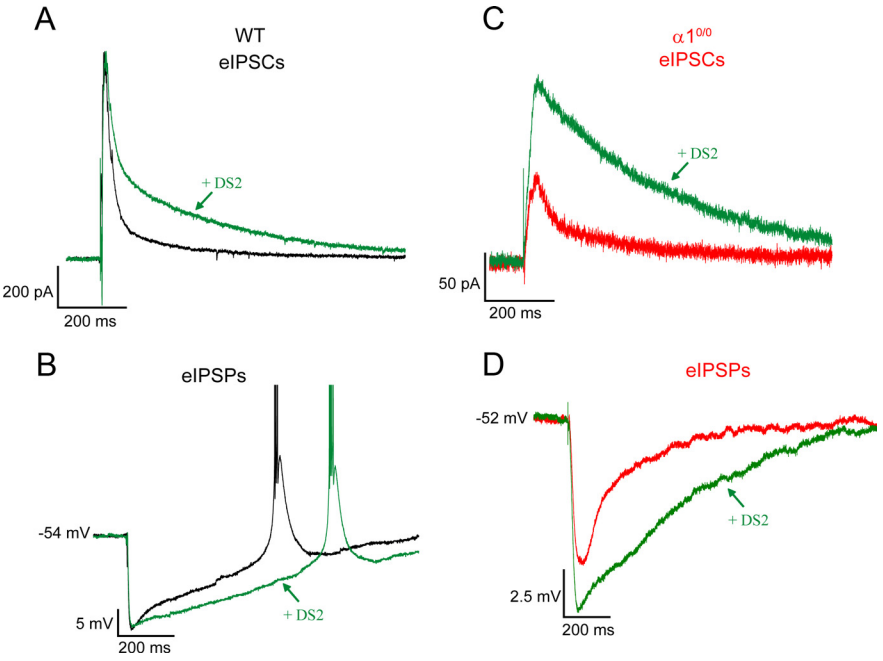

Figure 8. DS2 potentiates electrically evoked inhibition recorded from VB neurons of both WT and $\alpha1^{0/0}$ mice. ***A***, ***B***, Superimposed representative eIPSCs (***A***) and eIPSPs (***B***) recorded from WT VB neurons under control conditions (black) and after application of DS2 (green). ***C***, ***D***, Superimposed representative eIPSCs (***C***) and eIPSPs (***D***) recorded from $\alpha1^{0/0}$ VB neurons under control conditions (red) and after application of DS2 (green). Currents and potentials were evoked by extracellular stimulation of the nRT (single shocks, 20 μs duration).

Blockade of astrocytic GABA transporters prolongs the duration of bIPSCs and tIPSCs in an $\alpha4$ subunit-dependent manner

Clearance of synaptic GABA in the thalamus is primarily governed by the GABA transporters, GAT-1 and GAT-3 (De Biasi et al., 1998; Vitellaro-Zuccarello et al., 2003; Pow et al., 2005; Beenhakker and Huguenard, 2010). Thalamic GATs are exclusively astrocytic, where GAT-1 is located primarily in processes proximal to synaptic densities, whereas GAT-3 expression may be both proximal and distal to inhibitory synapses (De Biasi et al., 1998; Beenhakker and Huguenard, 2010). To investigate the role of thalamic GABA transporters in shaping the time course of burst- and tonic-mediated IPSCs, we tested the effect of nipecotic acid (1 mM), a nonselective blocker of GAT-1 and GAT-3, on nRT-VB pairs. Although no consistent effect was observed on bIPSC peak amplitude (Fig. 10*A*,*C*), nipecotic acid dramatically prolonged the decay time and increased the charge transfer of bIPSCs in response to comparable nRT spike bursts (Fig. 10*A*,*D*,*E*). Coapplication of 10 μM NO-711 (a selective GAT-1 blocker) and 30 μM SNAP-5114 (a selective GAT-3 blocker) produced similar effects on bIPSC decay time (τw percentage increase = 486 ± 52%, $n = 3$; compare nipecotic acid, τw percentage increase = 525 ± 71%). Deletion of the $\alpha4$ subunit abolished the effects of nipecotic acid (as observed with DS2) on bIPSC decay and charge transfer (Fig. 10*B*,*D*,*E*), apart from one example where nipecotic acid produced a clear, albeit limited, prolongation of bIPSC τw (% increase = 142%). In parallel with WT, nipecotic acid had no consistent effect on bIPSC peak amplitude (Fig. 10*C*). These experiments suggest that GABA transporters within the VB complex serve to limit the activation of presumably more distal eGABA$_A$Rs in response to the burst mode of GABA release.

We next investigated the effect of nipecotic acid on the tIPSC time course, and the nRT frequency-VB I_{hold} relationship. Nipecotic acid mimicked the effect of DS2, thus increasing fourfold

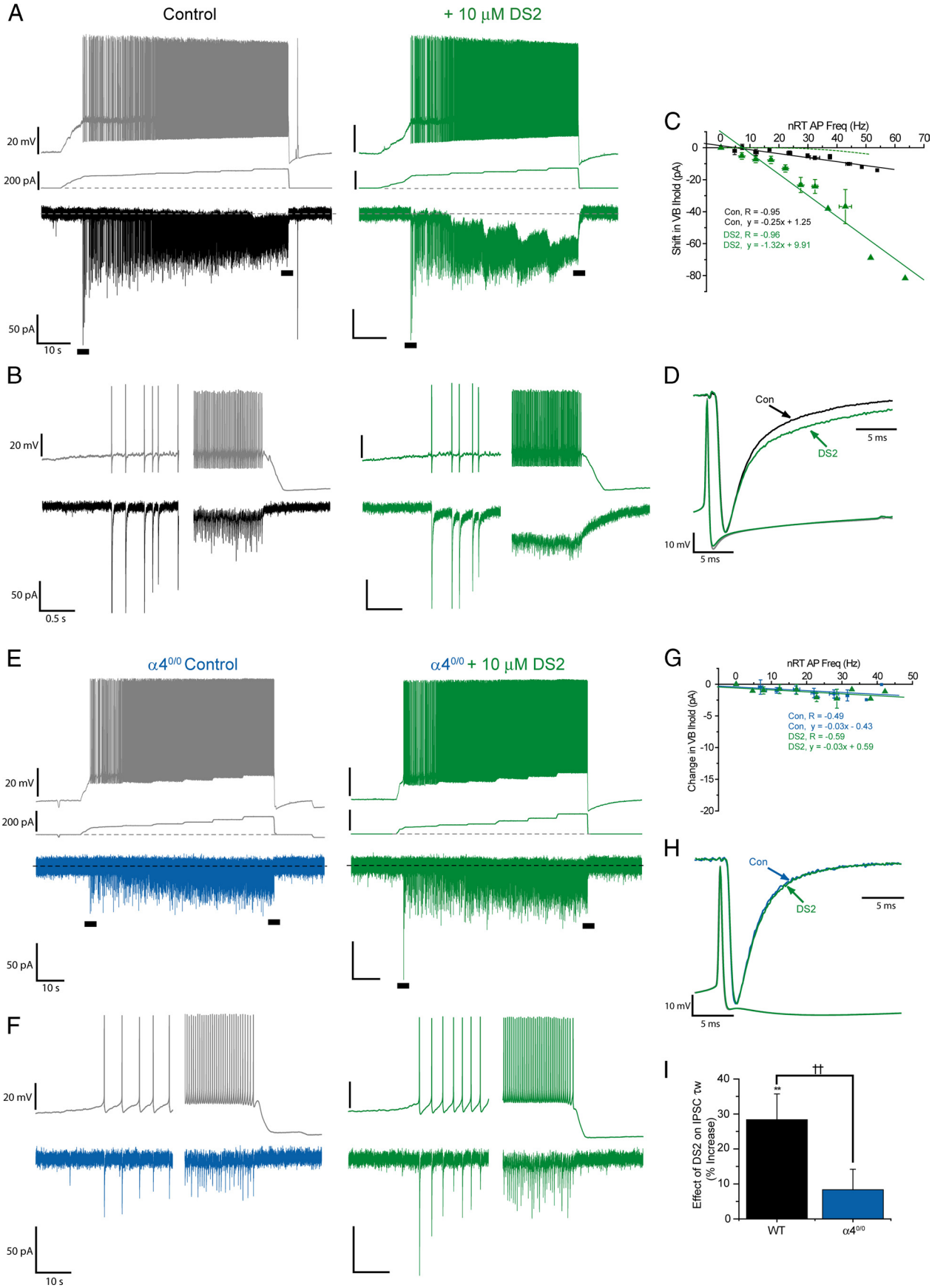

Figure 9. DS2 enhances the influence of nRT tonic firing on VB holding current. ***A***, Representative WT nRT-VB paired recording before (left, gray represents nRT; black represents VB) and after (right, green traces) application of 10 μM DS2. Top, nRT tonic spike train generated in response to incremental DC (middle). Bottom, Postsynaptic response (tIPSCs (*Figure legend continues.*)

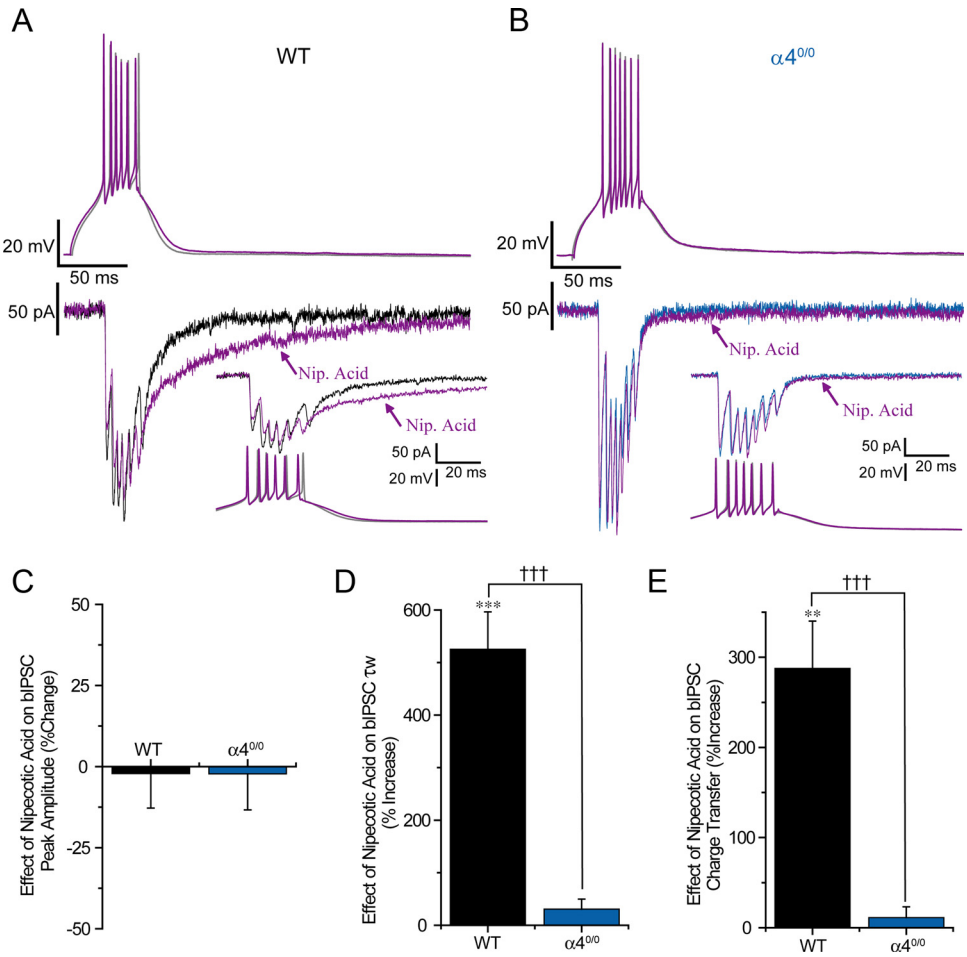

Figure 10. Nipecotic acid prolongs the duration of WT, but not $\alpha4^{0/0}$ bIPSCs in nRT-VB paired recordings. ***A***, ***B***, Representative paired nRT-VB recordings obtained from WT (***A***) and $\alpha4^{0/0}$ (***B***) mice before and after application of 1 mM nipecotic acid. Bottom, bIPSCs (black represents WT controls; blue represents $\alpha4^{0/0}$ controls; purple represents nipecotic acid) generated in response to presynaptic nRT spike bursts (top, gray represents control; purple represents nipecotic acid). The same traces are illustrated on an expanded time scale in the bottom inset, with the nRT traces now lowermost. ***C–E***, Summary bar graphs illustrating the effect of nipecotic acid on bIPSC peak amplitude (***C***) τw (***D***) and charge transfer (***E***) in WT (black bars, $n = 6$) and $\alpha4^{0/0}$ (blue bars, $n = 7$) paired recordings. $^{**}p < 0.01$ (one-way repeated-measures ANOVA). $^{***}p < 0.001$ (one-way repeated-measures ANOVA). ††† $p < 0.001$ versus WT (two-way repeated-measures ANOVA).

the slope of the linear regression fit to the frequency-I_{hold} plot (Fig. 11*A–C*). Indeed, a stepwise inward shift in VB I_{hold} was evident at the onset of each increment in nRT AP frequency. Moreover, nipecotic acid prolonged the tIPSC decay (in 5 of 6 pairs, assessed by the KS test of the tIPSC T50 distributions; data not shown; Fig. 11*D*,*I*). Deletion of the α4 subunit abolished the stepwise inward shift in tonic current evident for WT with nipecotic acid, such that the drug now had no effect on the linear regression fits to frequency-I_{hold} plots (Fig. 11*E–G*). Additionally, for $\alpha4^{0/0}$ neurons, the effect of nipecotic acid on the tIPSC decay was significantly reduced relative to WT (Fig. 11*H*,*I*). Collectively, these results suggest that perturbations in the normal function of thalamic GABA transporters, whether caused pharmacologically, or due to pathology (Cope et al., 2009), will impact on the kinetics and efficacy of relay neuron inhibition generated by burst and tonic modes of GABA release. The activity-dependent recruitment of additional α4βδ-GABA$_A$Rs underlies this effect.

←

(*Figure legend continued.*) and change in I_{hold}) to the presynaptic tonic train. Sections marked by black bars are expanded in ***B***. The first three tIPSCs are truncated. ***C***, Frequency-I_{hold} plot illustrating the correlation between nRT tonic AP frequency and VB I_{hold} before (black squares) and after (green triangles) application of DS2 (data plotted in 5 Hz bins; for details of plot construction, see Materials and Methods). Both datasets are fitted with a linear regression, with the linear equation and correlation coefficient for control and drug sections stated on the graph. Data derived from computer simulations (see Materials and Methods), incorporating a 28% prolongation of IPSC decay kinetics, are superimposed on the plot (green dotted line) to illustrate that enhanced IPSC summation is unlikely to account for the effect of DS2. ***D***, Superimposed, peak-scaled average tIPSCs and corresponding presynaptic APs obtained before (black represents VB; gray represents nRT) and after (green traces) application of DS2 in the pair illustrated in ***A***. ***E–H***, Representative paired nRT-VB recording obtained from an $\alpha4^{0/0}$ slice. Figure details are as described for WT in ***A–D***, except that $\alpha4^{0/0}$ VB traces in ***E***, ***F***, and ***H***, and symbols in ***G***, are blue. Horizontal dashed lines indicate pretonic train baseline levels. ***I***, Summary bar graph comparing the effect of DS2 on tIPSC τw in WT ($n = 6$) and $\alpha4^{0/0}$ ($n = 7$) pairs. $^{**}p < 0.01$ (one-way repeated-measures ANOVA). ††$p < 0.01$ versus WT (two-way repeated-measures ANOVA).

Discussion

In this study, we showed that the duration of burst-mediated IPSCs was greatly reduced by deletion of α4-containing eGABA$_A$Rs. Moreover, in recordings from $\alpha1^{0/0}$ VB neurons, which are devoid of synaptic GABA$_A$ receptors (Peden et al., 2008), we observed a robust residual eIPSC. Surprisingly, the decay time of IPSCs generated by tonic nRT discharge was also (modestly) reduced in $\alpha4^{0/0}$ pairs. Collectively, these observations provide evidence that extrasynaptic α4βδ-GABA$_A$Rs of VB neurons may be recruited by action potential-dependent GABA release from nRT terminals (see schematic illustration in Fig. 12).

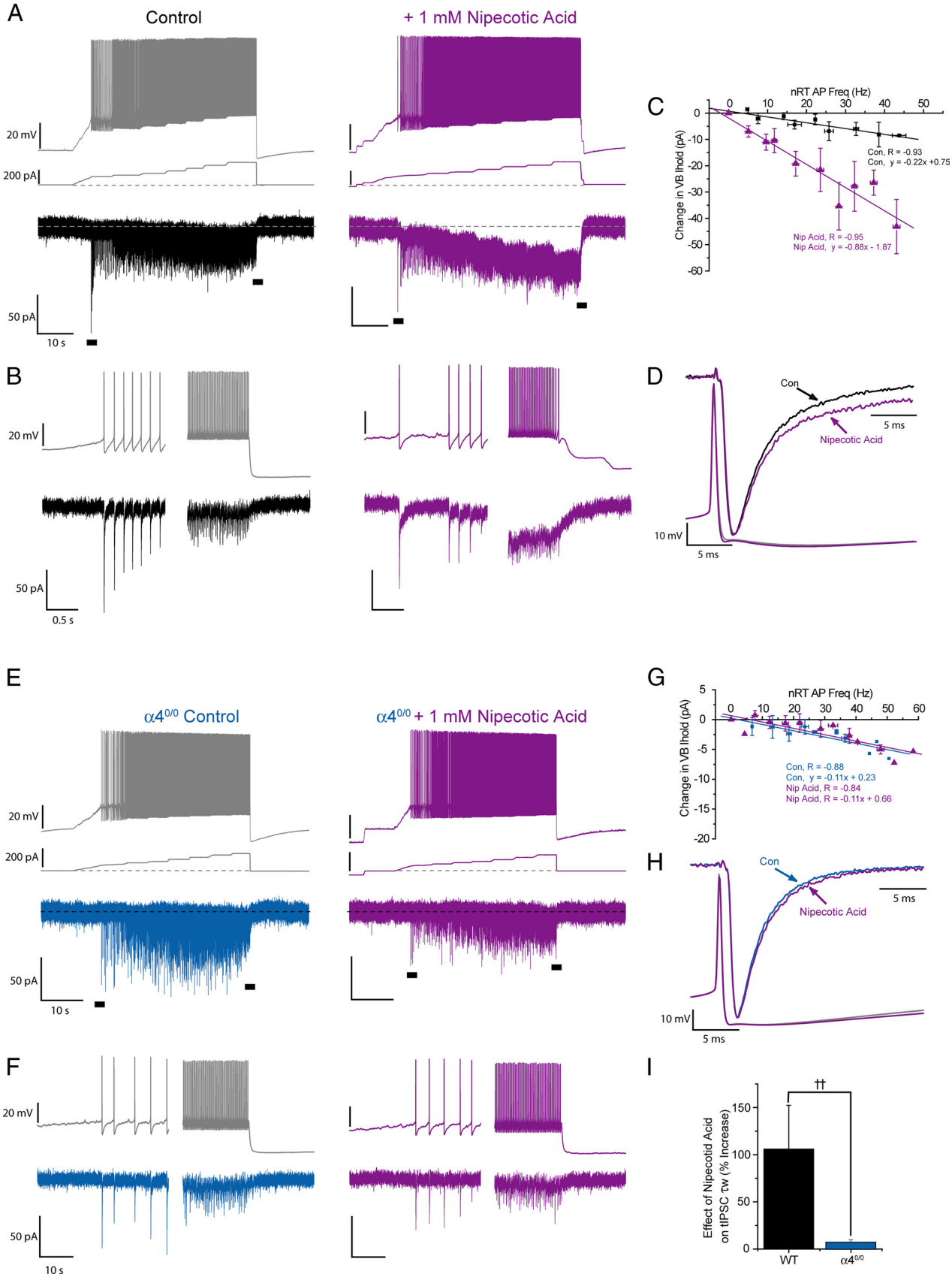

Figure 11. Blockade of GABA transport enhances the influence of nRT tonic firing on VB holding current in WT, but not $\alpha 4^{0/0}$ recordings. ***A***, WT nRT-VB paired recording before (left, gray for nRT, black for VB) and after (right, purple traces) nipecotic acid application (1 mM). Top, nRT tonic spike train generated in response to incremental DC (middle). Bottom, (*Figure legend continues.*)

Furthermore, DS2, a δ-selective positive allosteric modulator, greatly prolonged such events for WT, but not $\alpha4^{0/0}$ neurons. Thus, DS2 represents a new class of pharmacological tool to probe activity-dependent activation of eGABA$_A$Rs.

GABA spillover, wherein neurotransmitter diffuses beyond synaptic boundaries, influences the kinetics of inhibition at several, often unconventional synapses (Capogna and Pearce, 2011). The extrasynaptic location, apparent high affinity for GABA, and limited desensitization of $\alpha4\beta\delta$ and $\alpha6\beta\delta$ receptors have supported the view that spillover inhibition is mediated by δ-GABA$_A$Rs (Wei et al., 2003; Farrant and Nusser, 2005). However, this view has been challenged because, at physiological temperatures, recombinant δ-GABA$_A$Rs exhibit greater desensitization in the presence of ambient-like concentrations of GABA than "synaptic" receptor isoforms, thus limiting their responsiveness to phasic-like GABA transients (Bright et al., 2011). In agreement, expression of slow sIPSCs in X-type neurons of both dorsal and ventral lateral geniculate nucleus (LGN) does not correlate with δ subunit expression, which is restricted to the dLGN (Bright et al., 2011). Nevertheless, the briefer decay of evoked, burst-, and tonic-mediated IPSCs recorded from $\alpha4^{0/0}$ tissue at, or near, physiological temperatures, demonstrates that in the VB, $\alpha4\beta2\delta$ receptors are in a sufficiently nondesensitized state to be gated in a phasic manner by both burst and tonic modes of transmitter release. Similarly, at near physiological temperature, δ-GABA$_A$Rs mediate a spillover component of dendritic eIPSCs recorded from dentate granule cells (Wei et al., 2003) and influence the kinetics of slow IPSCs generated at neurogliaform-pyramidal cell synapses (Szabadics et al., 2007; Oláh et al., 2009). By contrast, deletion of the δ subunit does not influence the spillover component of cerebellar granule cell sIPSCs (Bright et al., 2011). Thus, the molecular composition of receptors responsible for spillover inhibition appears to vary, depending on the synapse (see below). As noted above, recombinant experiments have indicated a substantial degree of desensitization of δ-GABA$_A$Rs on continued exposure to "ambient" GABA concentrations that should preclude their activation by phasic transmitter spillover (Mortensen et al., 2010; Bright et al., 2011). However, the spatiotemporal profile of transmitter presentation to recombinantly expressed receptors is unlikely to completely reproduce that experienced by VB δ-GABA$_A$Rs during nRT bursts or tonic trains. In addition, the kinetic properties of GABA$_A$Rs retained within excised membrane patches from non-neuronal cell lines may not completely reflect those of identical native receptors (e.g., compare Tia et al., 1996 with Nusser et al., 1997). Such differences have been proposed to occur because of the lack of intracellular regulatory elements normally present within a native neuronal environment (e.g., associated proteins, cytoskeletal elements, and regulatory enzymes, such as those responsible for phosphorylation), which are known to influence receptor function in a neuron-selective fashion (Nusser et al., 1999; Jacob et al., 2008).

GABA spillover generates unusually slow IPSCs (termed GABA$_{A,slow}$) at neurogliaform-principle cell connections (Szabadics et al., 2007; Karayannis et al., 2010; Manko et al., 2012). At this anatomically unconventional synapse, a diffuse, long-lived GABA transient, of relatively low concentration, partly underlies the kinetic properties of GABA$_{A,slow}$. In the cerebellum, GABA$_A$R-mediated spillover inhibition of granule cells plays an important role in network computational processes (Rossi and Hamann, 1998; Mitchell and Silver, 2000; Hamann et al., 2002). Here, the retention of Golgi cell axons and granule cell dendrites within a glial-ensheathed glomerulus apparently favors spillover inhibition. Relay neurons of some thalamic nuclei, particularly within the dLGN, also express glomerular synapses (Sherman and Guillery, 2001), which are thought to underlie a subpopulation of slow sIPSCs (Bright et al., 2011). However, the dLGN glomerular synapse is distinct from the nRT-VB synapse studied here because inhibitory terminals within dLGN glomeruli are derived from local interneurons. In rodents, interneurons are virtually absent from all other relay nuclei, including VB (Sherman and Guillery, 2001). Moreover, the axonal terminals of rat nRT neurons are exclusively extraglomerular in VB and dLGN (Montero and Scott, 1981; Peschanski et al., 1983). Nevertheless, despite the absence of a morphological specialization favoring neurotransmitter pooling, we still observed a presumed spillover component of IPSCs generated by physiologically relevant presynaptic activity.

GABA transporters are commonly assumed to function at maximum capacity to rapidly terminate inhibition. However, at normal resting potentials, GATs operate at near equilibrium and may even reverse direction (Richerson and Wu, 2003). Thus, the equilibrium state of GATs determines not only the efficiency of GABA clearance, but also ambient GABA concentrations. Although not directly tested, the presumed spillover component of bIPSC and tIPSCs implies that the elevated GABA levels achieved during action potential-dependent release are sufficient to overwhelm the inward transport capacity of thalamic GATs. Nevertheless, their importance in limiting the diffusional spread of GABA beyond synaptic boundaries, is supported by the observation that GAT blockade dramatically prolonged bIPSCs and tIPSCs while also strengthening the relationship between presynaptic tonic firing and postsynaptic tonic current amplitude. Thus, blocking GAT function probably allows GABA to diffuse further from release sites, thus facilitating recruitment of more distal eGABA$_A$Rs. Although the effects of GAT antagonists vary depending on the preparation, cell type, and phasic event studied (i.e., mIPSC, sIPSC, eIPSC), GAT blockade has been shown to prolong the decay of "fast" inhibition in some studies, particularly when multiple inputs are activated (Roepstorff and Lambert, 1992, 1994; Draguhn and Heinemann, 1996; Nusser et al., 2001; Overstreet and Westbrook, 2003; Keros and Hablitz, 2005). The importance of a functional thalamic GABA transport system is emphasized by the observation that GAT-1 function is compromised across multiple rodent models of absence seizures, resulting in upregulated relay cell tonic inhibition (Cope et al., 2009; Pirttimaki et al., 2012). As rhythmic burst firing is a prevailing feature of nRT neurons during spike-wave discharges (Pinault et al., 1998; Slaght et al., 2002), our results suggest that perturbations of GABA transport would also influence the dura-

←

(*Figure legend continued.*) Postsynaptic response (tIPSCs and change in I_{hold}) to the presynaptic tonic train. Sections marked by black bars are expanded in ***B***. The first tIPSCs are truncated. ***C***, Frequency-I_{hold} plot illustrating the correlation between nRT AP frequency and VB I_{hold} before (black squares) and after (purple triangles) nipecotic acid application (data plotted in 5 Hz bins; for details of plot construction, see Materials and Methods). Both datasets are fitted with a linear regression, with the equation and correlation coefficient for control and drug sections stated on the graph. ***D***, Superimposed, peak scaled average tIPSCs and corresponding presynaptic APs obtained before (black for VB, gray for nRT) and after (purple traces) application of nipecotic acid from the pair illustrated in ***A***. ***E–H***, Paired $\alpha4^{0/0}$ recording obtained before and after nipecotic acid. Figure details are as described for WT in ***A–D***, except that control $\alpha4^{0/0}$ VB traces in ***E***, ***F***, and ***H***, and symbols in ***G***, are blue. Horizontal dashed lines indicate pretonic train baseline levels. ***I***, Summary bar graph comparing the effect of nipecotic acid on tIPSC τw in WT (black, $n = 6$) and $\alpha4^{0/0}$ (blue, $n = 7$) pairs. ††$p < 0.01$ versus WT, two-way repeated-measures ANOVA.

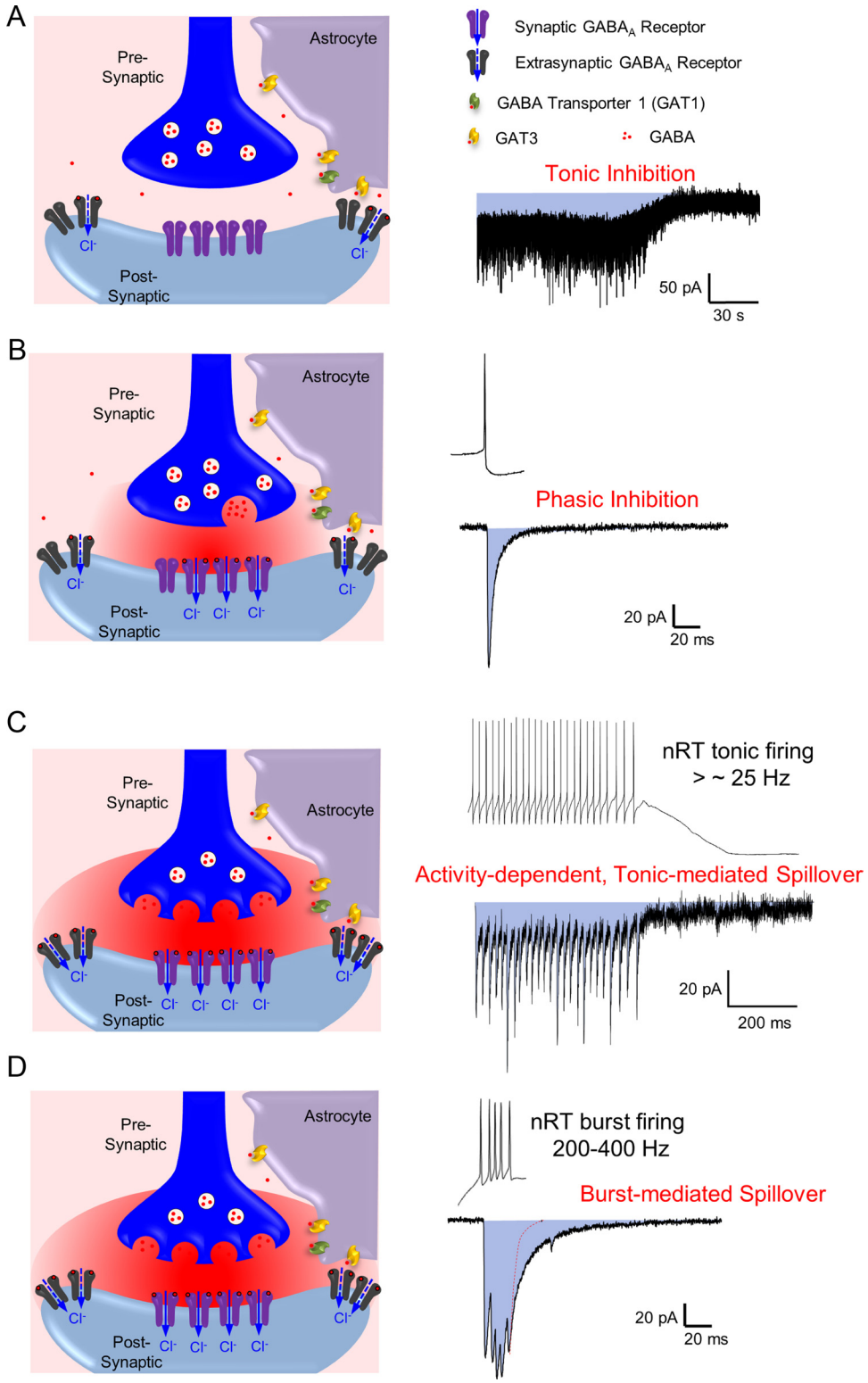

Figure 12. Summary schematic illustrating the range of inhibitory modes occurring at the nRT-VB synapse. ***A–D***, The hypothetical diagrams in the left-hand column depict synaptic GABA transients (illustrated by red dots and/or a graded red cloud) generated in response to increasingly intense nRT discharge frequencies as depicted in the upper right-hand panels (except ***A***). Lower right panels, Inhibitory, GABA$_A$R-mediated responses of VB neurons corresponding to each level of presynaptic activity. Light blue shaded regions in each VB trace represent the inhibitory charge imposed by each level of nRT activity. The symbol key in ***A*** is also applicable to ***B–D***. In VB, tonic inhibition (***A***), mediated by eGABA$_A$Rs, is not dependent on action potential-mediated GABA release, although ongoing spontaneous GABA release (see the miniature IPSCs in the trace) may conceivably contribute to the maintenance of tonic inhibition. Our results suggest that, during action potential-dependent phasic inhibition (***B***), sufficient GABA may diffuse to perisynaptic regions to activate $\alpha4\beta\delta$-GABA$_A$Rs, thus producing a modest increase in IPSC decay time. However, at higher nRT tonic firing frequencies, the sustained release of GABA further enhances the recruitment of $\alpha4$-GABA$_A$Rs (***C***), thus potentiating baseline tonic inhibition. Therefore, the magnitude of VB neuron tonic inhibition may fluctuate according to the intensity of nRT tonic firing. Finally, during intermittent burst firing (intraburst frequency $>$200 Hz), "spillover" of GABA into perisynaptic/extrasynaptic domains (***D***) recruits multiple $\alpha4\beta\delta$-GABA$_A$Rs, thereby doubling the decay time constant of burst-mediated IPSCs. The dashed red line superimposed on the trace in ***D*** indicates the decay phase of the IPSC in ***B*** (recorded from the same pair), emphasizing the prolonged IPSC decay kinetics generated by "burst-mediated spillover."

tion of phasic eGABA$_A$R-mediated inhibition during absence seizures. Such a hypothesis will have important implications for the overall function of the thalamocortical loop during absence seizure generation (Crunelli and Leresche, 2002).

Reciprocal connections between nRT and relay nuclei, together with several intrinsic voltage-dependent conductances, engender the thalamus with an ability to generate, or propagate, many behavior- and sleep-related oscillations (Steriade, 2003). Within this network, the amplitude and duration of relay neuron IPSPs have been suggested to define the period and synchrony of some TC oscillations, principally by controlling the timing of postinhibitory rebound bursts (Kim et al., 1997; Huguenard and McCormick, 2007). Thus, prolonged bIPSCs induced by phasic activation of eGABA$_A$Rs could simplistically impose a delay in rebound burst onset, thereby lengthening the period of rebound-dependent oscillations. In agreement, the T50 of eIPSPs recorded from $\alpha4^{0/0}$ and $\delta^{0/0}$ VB neurons was approximately halved. However, the association between IPSP duration and rebound burst timing is not simply linear, due to the complex activation kinetics of the IPSP-triggered intrinsic conductances (e.g., I_h and I_T). Indeed, a study of postinhibitory rebound properties and spindle-like oscillations in mouse thalamocortical slices demonstrated that, although modest increases in IPSC decay time increases the probability of firing rebound bursts, such changes can paradoxically shorten rebound latency and decrease network synchrony (Sohal et al., 2006). Furthermore, given the voltage dependence of intrinsic conductances in TC neurons, the membrane potential preceding the IPSP can further influence rebound burst timing and synchrony (Sohal et al., 2006). In agreement, increasing the tonic conductance of dLGN neurons increases the timing variability of rebound bursts (Bright et al., 2007). Thus, predicting the impact of spillover activation of eGABA$_A$Rs, which can vary significantly between nRT-VB connections (see Fig. 3*D*), is not straightforward. Importantly, GABA$_B$R activation may further influence the properties of inhibition at the nRT-VB synapse (Beenhakker and Huguenard, 2010; Connelly et al., 2013). Incorporation of our results into simulated network models (Destexhe, 1999) may help to elucidate the relative contribution of ionotropic and metabotropic inhibitory mechanisms to TC network function.

In nRT-VB pairs, we observed a direct relationship between presynaptic tonic firing frequency and postsynaptic holding current, which was dramatically enhanced in the presence of DS2 or nipecotic acid. These results predict that VB neuron membrane potential can be dynamically influenced by nRT output, on a time scale that extends beyond the brief coincidence between a presynaptic spike and its associated IPSP. Furthermore, this occurs in addition to the baseline tonic conductance, which, in VB, persists in the presence of tetrodotoxin (Cope et al., 2005, 2009). Importantly, elevating tonic inhibition using the δ-preferring agonist, THIP, can promote the switch from tonic to burst firing by inducing a hyperpolarizing shift in membrane potential (Cope et al., 2005). Thus, an activity-dependent regulation of tonic inhibition may similarly influence membrane potential and, by extension, transitions between tonic and burst firing. However, shunting inhibition generated by the tonic conductance exerts powerful, cell-specific effects on the integrative properties of neurons and networks (Mitchell and Silver, 2003; Pavlov et al., 2009; Duguid et al., 2012). Thus, if VB tonic inhibition is flexible under varying nRT output, this will presumably influence the computational properties of VB neurons by modifying their excitatory input sensitivity (altered gain function) and/or the threshold for action potential firing in response to synaptic excitation (shifted offset) (Mitchell and Silver, 2003; Semyanov et al., 2004; Pavlov et al., 2009). Moreover, such changes will be magnified under circumstances favoring phasic spillover activation of eGABA$_A$Rs (e.g., perturbed GABA uptake) (Cope et al., 2009) or in the presence of δ-selective modulators (Jensen et al., 2013).

In conclusion, we have shown that extrasynaptic $\alpha4\beta\delta$-GABA$_A$Rs in the somatosensory thalamus are not merely passive sensors of ambient GABA but may also dynamically modulate neuronal inhibition by "sensing" presynaptic activity levels. Moreover, we demonstrate that eGABA$_A$Rs sculpt the time course of IPSCs generated in response to burst and tonic spike activity in nRT neurons. Furthermore, the sensitivity of burst- and tonic-mediated IPSCs to manipulation of GAT function, or modulation of eGABA$_A$Rs, provides novel therapeutic opportunities for treatment of disorders linked to dysfunction of the thalamocortical system. Given the importance of the nRT-relay neuron synapse for generation of synchronous, state-dependent oscillations within the thalamocortical network, these results emphasize that eGABA$_A$Rs serve a more complex purpose within somatosensory thalamus than simple provision of static "shunting" inhibition. Indeed, this hypothesis is supported by recent work demonstrating that spindle and cortical slow oscillations are relatively unaffected by virus-mediated focal excision of synaptic γ2-GABA$_A$Rs from relay cells of the VPM (Mátyás et al., 2012; L. Acsády and A. Lüthi, personal communication). Specifically, although VPM sIPSCs are abolished by focal deletion of the γ2 subunit, a slowly rising and decaying burst-mediated current remains in the absence of synaptic receptors (reminiscent of our observations in $\alpha1^{0/0}$ mice), which unexpectedly seems to be sufficient to preserve relatively normal network function (Mátyás et al., 2012; Rovo et al., 2012). Collectively, these observations suggest that the general view of synaptic and extrasynaptic GABA$_A$ receptors as functionally separate entities should be revised.

References

Avanzini G, de Curtis M, Panzica F, Spreafico R (1989) Intrinsic properties of nucleus reticularis thalami neurones of the rat studied in vitro. J Physiol 416:111–122. Medline

Beenhakker MP, Huguenard JR (2010) Astrocytes as gatekeepers of GABA$_B$ receptor function. J Neurosci 30:15262–15276. CrossRef Medline

Belelli D, Peden DR, Rosahl TW, Wafford KA, Lambert JJ (2005) Extrasynaptic GABA$_A$ receptors of thalamocortical neurons: a molecular target for hypnotics. J Neurosci 25:11513–11520. CrossRef Medline

Bessaïh T, Bourgeais L, Badiu CI, Carter DA, Toth TI, Ruano D, Lambolez B, Crunelli V, Leresche N (2006) Nucleus-specific abnormalities of GABAergic synaptic transmission in a genetic model of absence seizures. J Neurophysiol 96:3074–3081. CrossRef Medline

Brickley SG, Revilla V, Cull-Candy SG, Wisden W, Farrant M (2001) Adaptive regulation of neuronal excitability by a voltage-independent potassium conductance. Nature 409:88–92. CrossRef Medline

Bright DP, Aller MI, Brickley SG (2007) Synaptic release generates a tonic GABA$_A$ receptor-mediated conductance that modulates burst precision in thalamic relay neurons. J Neurosci 27:2560–2569. CrossRef Medline

Bright DP, Renzi M, Bartram J, McGee TP, MacKenzie G, Hosie AM, Farrant M, Brickley SG (2011) Profound desensitization by ambient GABA limits activation of δ-containing GABA$_A$ receptors during spillover. J Neurosci 31:753–763. CrossRef Medline

Capogna M, Pearce RA (2011) GABA$_{A,slow}$: causes and consequences. Trends Neurosci 34:101–112. CrossRef Medline

Chandra D, Jia F, Liang J, Peng Z, Suryanarayanan A, Werner DF, Spigelman I, Houser CR, Olsen RW, Harrison NL, Homanics GE (2006) GABA$_A$ receptor α4 subunits mediate extrasynaptic inhibition in thalamus and dentate gyrus and the action of gaboxadol. Proc Natl Acad Sci U S A 103:15230–15235. CrossRef Medline

Connelly WM, Fyson SJ, Errington AC, McCafferty CP, Cope DW, Di Gio-

vanni G, Crunelli V (2013) GABAB receptors regulate extrasynaptic GABAA receptors. J Neurosci 33:3780–3785. CrossRef Medline

Cope DW, Hughes SW, Crunelli V (2005) $GABA_A$ receptor-mediated tonic inhibition in thalamic neurons. J Neurosci 25:11553–11563. CrossRef Medline

Cope DW, Di Giovanni G, Fyson SJ, Orbán G, Errington AC, Lorincz ML, Gould TM, Carter DA, Crunelli V (2009) Enhanced tonic $GABA_A$ inhibition in typical absence epilepsy. Nat Med 15:1392–1398. CrossRef Medline

Cox CL, Huguenard JR, Prince DA (1997) Nucleus reticularis neurons mediate diverse inhibitory effects in thalamus. Proc Natl Acad Sci U S A 94:8854–8859. CrossRef Medline

Crunelli V, Leresche N (2002) Childhood absence epilepsy: genes, channels, neurons and networks. Nat Rev Neurosci 3:371–382. CrossRef Medline

Crunelli V, Lightowler S, Pollard CE (1989) A T-type Ca^{2+} current underlies low-threshold Ca^{2+} potentials in cells of the cat and rat lateral geniculate nucleus. J Physiol 413:543–561. Medline

De Biasi S, Vitellaro-Zuccarello L, Brecha NC (1998) Immunoreactivity for the GABA transporter-1 and GABA transporter-3 is restricted to astrocytes in the rat thalamus: a light and electron-microscopic immunolocalization. Neuroscience 83:815–828. CrossRef Medline

Destexhe A (1999) Can $GABA_A$ conductances explain the fast oscillation frequency of absence seizures in rodents? Eur J Neurosci 11:2175–2181. CrossRef Medline

Draguhn A, Heinemann U (1996) Different mechanisms regulate IPSC kinetics in early postnatal and juvenile hippocampal granule cells. J Neurophysiol 76:3983–3993. Medline

Duguid I, Branco T, London M, Chadderton P, Häusser M (2012) Tonic inhibition enhances fidelity of sensory information transmission in the cerebellar cortex. J Neurosci 32:11132–11143. CrossRef Medline

Evrard A, Ropert N (2009) Early development of the thalamic inhibitory feedback loop in the primary somatosensory system of the newborn mice. J Neurosci 29:9930–9940. CrossRef Medline

Farrant M, Nusser Z (2005) Variations on an inhibitory theme: phasic and tonic activation of $GABA_A$ receptors. Nat Rev Neurosci 6:215–229. CrossRef Medline

Gentet LJ, Ulrich D (2003) Strong, reliable and precise synaptic connections between thalamic relay cells and neurones of the nucleus reticularis in juvenile rats. J Physiol 546:801–811. CrossRef Medline

Hamann M, Rossi DJ, Attwell D (2002) Tonic and spillover inhibition of granule cells control information flow through cerebellar cortex. Neuron 33:625–633. CrossRef Medline

Herd MB, Foister N, Chandra D, Peden DR, Homanics GE, Brown VJ, Balfour DJ, Lambert JJ, Belelli D (2009) Inhibition of thalamic excitability by 4,5,6,7-tetrahydroisoxazolo[4,5-c]pyridine-3-ol: a selective role for δ-$GABA_A$ receptors. Eur J Neurosci 29:1177–1187. CrossRef Medline

Houston CM, Bright DP, Sivilotti LG, Beato M, Smart TG (2009) Intracellular chloride ions regulate the time course of GABA-mediated inhibitory synaptic transmission. J Neurosci 33:10416–10423. CrossRef Medline

Huguenard JR, McCormick DA (2007) Thalamic synchrony and dynamic regulation of global forebrain oscillations. Trends Neurosci 30:350–356. CrossRef Medline

Jacob TC, Moss SJ, Jurd R (2008) GABA(A) receptor trafficking and its role in the dynamic modulation of neuronal inhibition. Nat Rev Neurosci 9:331–343. CrossRef Medline

Jahnsen H, Llinás R (1984) Electrophysiological properties of guinea-pig thalamic neurones: an in vitro study. J Physiol 349:205–226. Medline

Jensen ML, Wafford KA, Brown AR, Belelli D, Lambert JJ, Mirza NR (2013) The δ selective compound 2 (DS2): a detailed study of subunit selectivity, mechanism and site of action utilising human recombinant and rodent native $GABA_A$ receptors. Br J Pharmacol 168:1118–1132. CrossRef Medline

Jia F, Pignataro L, Schofield CM, Yue M, Harrison NL, Goldstein PA (2005) An extrasynaptic $GABA_A$ receptor mediates tonic inhibition in thalamic VB neurons. J Neurophysiol 94:4491–4501. CrossRef Medline

Jia F, Pignataro L, Harrison NL (2007) $GABA_A$ receptors in the thalamus: α4 subunit expression and alcohol sensitivity. Alcohol 41:177–185. CrossRef Medline

Karayannis T, Elfant D, Huerta-Ocampo I, Teki S, Scott RS, Rusakov DA, Jones MV, Capogna M (2010) Slow GABA transient and receptor desensitization shape synaptic responses evoked by hippocampal neurogliaform cells. J Neurosci 30:9898–9909. CrossRef Medline

Keros S, Hablitz JJ (2005) Subtype-specific GABA transporter antagonists synergistically modulate phasic and tonic $GABA_A$ conductances in rat neocortex. J Neurophysiol 94:2073–2085. CrossRef Medline

Kim U, Sanchez-Vives MV, McCormick DA (1997) Functional dynamics of GABAergic inhibition in the thalamus. Science 278:130–134. CrossRef Medline

Kralic JE, Sidler C, Parpan F, Homanics GE, Morrow AL, Fritschy JM (2006) Compensatory alteration of inhibitory synaptic circuits in cerebellum and thalamus of gamma-aminobutyric acid type A receptor α1 subunit knockout mice. J Comp Neurol 495:408–421. CrossRef Medline

Lam YW, Sherman SM (2005) Mapping by laser photostimulation of connections between the thalamic reticular and ventral posterior lateral nuclei in the rat. J Neurophysiol 94:2472–2483. CrossRef Medline

Mañko M, Bienvenu TC, Dalezios Y, Capogna M (2012) Neurogliaform cells of amygdala: a source of slow phasic inhibition in the basolateral complex. J Physiol 590:5611–5627. CrossRef Medline

Mátyás F, Slézia A, Rovó Z, Barthó P, Hangya B, Lüthi A, Acsády L (2012) Cellular and network effects of pharmaco-genetic deletion of synaptic GABA-A receptors in the mouse somatosensory thalamus. FENS Abstr 6:004.25.

Mihalek RM, Banerjee PK, Korpi ER, Quinlan JJ, Firestone LL, Mi ZP, Lagenaur C, Tretter V, Sieghart W, Anagnostaras SG, Sage JR, Fanselow MS, Guidotti A, Spigelman I, Li Z, DeLorey TM, Olsen RW, Homanics GE (1999) Attenuated sensitivity to neuroactive steroids in gamma-aminobutyrate type A receptor δsubunit knockout mice. Proc Natl Acad Sci U S A 96:12905–12910. CrossRef Medline

Mitchell SJ, Silver RA (2000) GABA spillover from single inhibitory axons suppresses low-frequency excitatory transmission at the cerebellar glomerulus. J Neurosci 20:8651–8658. Medline

Mitchell SJ, Silver RA (2003) Shunting inhibition modulates neuronal gain during synaptic excitation. Neuron 38:433–445. CrossRef Medline

Montero VM, Scott GL (1981) Synaptic terminals in the dorsal lateral geniculate nucleus from neurons of the thalamic reticular nucleus: a light and electron microscope autoradiographic study. Neuroscience 6:2561–2577. CrossRef Medline

Mortensen M, Ebert B, Wafford K, Smart TG (2010) Distinct activities of GABA agonists at synaptic- and extrasynaptic-type GABAA receptors. J Physiol 588:1251–1268. CrossRef Medline

Nusser Z, Cull-Candy S, Farrant M (1997) Differences in synaptic GABA(A) receptor number underlie variation in GABA mini amplitude. Neuron 19:697–709. CrossRef Medline

Nusser Z, Sieghart W, Mody I (1999) Differential regulation of synaptic GABAA receptors by cAMP-dependent protein kinase in mouse cerebellar and olfactory bulb neurones. J Physiol 521:421–435. CrossRef Medline

Nusser Z, Naylor D, Mody I (2001) Synapse-specific contribution of the variation of transmitter concentration to the decay of inhibitory postsynaptic currents. Biophys J 80:1251–1261. CrossRef Medline

Oláh S, Füle M, Komlósi G, Varga C, Báldi R, Barzó P, Tamás G (2009) Regulation of cortical microcircuits by unitary GABA-mediated volume transmission. Nature 461:1278–1281. CrossRef Medline

Overstreet LS, Westbrook GL (2003) Synapse density regulates independence at unitary inhibitory synapses. J Neurosci 23:2618–2626. Medline

Pavlov I, Savtchenko LP, Kullmann DM, Semyanov A, Walker MC (2009) Outwardly rectifying tonically active $GABA_A$ receptors in pyramidal cells modulate neuronal offset, not gain. J Neurosci 29:15341–15350. CrossRef Medline

Paxinos G, Franklin KBJ (2013) The mouse brain in stereotaxic coordinates, Ed 4. New York: Elsevier.

Peden DR, Petitjean CM, Herd MB, Durakoglugil MS, Rosahl TW, Wafford K, Homanics GE, Belelli D, Fritschy JM, Lambert JJ (2008) Developmental maturation of synaptic and extrasynaptic $GABA_A$ receptors in mouse thalamic ventrobasal neurones. J Physiol 586:965–987. CrossRef Medline

Peschanski M, Ralston HJ, Roudier F (1983) Reticularis thalami afferents to the ventrobasal complex of the rat thalamus: an electron microscope study. Brain Res 270:325–329. CrossRef Medline

Pinault D (2011) Dysfunctional thalamus-related networks in schizophrenia. Schizophr Bull 37:238–243. CrossRef Medline

Pinault D, Leresche N, Charpier S, Deniau JM, Marescaux C, Vergnes M, Crunelli V (1998) Intracellular recordings in thalamic neurones during spontaneous spike and wave discharges in rats with absence epilepsy. J Physiol 509:449–456. CrossRef Medline

Pirttimaki T, Parri HR, Crunelli V (2013) Astrocytic GAT-1 dysfunction in experimental absence seizures. J Physiol 591:823–833. CrossRef Medline

Pow DV, Sullivan RK, Williams SM, Scott HL, Dodd PR, Finkelstein D (2005) Differential expression of the GABA transporters GAT-1 and GAT-3 in brains of rats, cats, monkeys and humans. Cell Tissue Res 320:379–392. CrossRef Medline

Richerson GB, Wu Y (2003) Dynamic equilibrium of neurotransmitter transporters: not just for reuptake anymore. J Neurophysiol 90:1363–1374. CrossRef Medline

Roepstorff A, Lambert JD (1992) Comparison of the effect of the GABA uptake blockers, tiagabine and nipecotic acid, on inhibitory synaptic efficacy in hippocampal CA1 neurones. Neurosci Lett 146:131–134. CrossRef Medline

Roepstorff A, Lambert JD (1994) Factors contributing to the decay of the stimulus-evoked IPSC in rat hippocampal CA1 neurons. J Neurophysiol 72:2911–2926. Medline

Rossi DJ, Hamann M (1998) Spillover-mediated transmission at inhibitory synapses promoted by high affinity α6 subunit GABA$_A$ receptors and glomerular geometry. Neuron 20:783–795. CrossRef Medline

Rovo Z, Mátyás F, Lüthi A, Acsády L (2012) Molecular dissection of GABA-A receptor-mediated inhibition in mouse thalamocortical cells. FENS Abstr 6:004.29.

Semyanov A, Walker MC, Kullmann DM, Silver RA (2004) Tonically active GABA$_A$ receptors: modulating gain and maintaining the tone. Trends Neurosci 27:262–269. CrossRef Medline

Sherman SM, Guillery RW (2001) Exploring the thalamus. San Diego: Academic.

Slaght SJ, Leresche N, Deniau JM, Crunelli V, Charpier S (2002) Activity of thalamic reticular neurons during spontaneous genetically determined spike and wave discharges. J Neurosci 22:2323–2334. Medline

Sohal VS, Pangratz-Fuehrer S, Rudolph U, Huguenard JR (2006) Intrinsic and synaptic dynamics interact to generate emergent patterns of rhythmic bursting in thalamocortical neurons. J Neurosci 26:4247–4255. CrossRef Medline

Steriade M (2003) Neuronal substrates of sleep and epilepsy. Cambridge: Cambridge UP.

Stórustovu SI, Ebert B (2006) Pharmacological characterization of agonists at δ-containing GABAA receptors: functional selectivity for extrasynaptic receptors is dependent on the absence of gamma2. J Pharmacol Exp Ther 316:1351–1359. CrossRef Medline

Sun C, Mtchedlishvili Z, Erisir A, Kapur J (2007) Diminished neurosteroid sensitivity of synaptic inhibition and altered location of the α4 subunit of GABA$_A$ receptors in an animal model of epilepsy. J Neurosci 27:12641–12650. CrossRef Medline

Sur C, Farrar SJ, Kerby J, Whiting PJ, Atack JR, McKernan RM (1999) Preferential coassembly of α4 and δ subunits of the gamma-aminobutyric acidA receptor in rat thalamus. Mol Pharmacol 56:110–115. Medline

Sur C, Wafford KA, Reynolds DS, Hadingham KL, Bromidge F, Macaulay A, Collinson N, O'Meara G, Howell O, Newman R, Myers J, Atack JR, Dawson GR, McKernan RM, Whiting PJ, Rosahl TW (2001) Loss of the major GABA$_A$ receptor subtype in the brain is not lethal in mice. J Neurosci 21:3409–3418. Medline

Szabadics J, Tamás G, Soltesz I (2007) Different transmitter transients underlie presynaptic cell type specificity of GABA$_A$, slow and GABA$_A$, fast. Proc Natl Acad Sci U S A 104:14831–14836. CrossRef Medline

Tia S, Wang JF, Kotchabhakdi N, Vicini S (1996) Distinct deactivation and desensitization kinetics of recombinant GABAA receptors. Neuropharmacology 35:1375–1382. CrossRef Medline

Timofeev I (2011) Neuronal plasticity and thalamocortical sleep and waking oscillations. Prog Brain Res 193:121–144. CrossRef Medline

Ulrich D, Huguenard JR (1996) GABAB receptor-mediated responses in GABAergic projection neurones of rat nucleus reticularis thalami in vitro. J Physiol 493:845–854. Medline

Vitellaro-Zuccarello L, Calvaresi N, De Biasi S (2003) Expression of GABA transporters, GAT-1 and GAT-3, in the cerebral cortex and thalamus of the rat during postnatal development. Cell Tissue Res 313:245–257. CrossRef Medline

von Krosigk M, Bal T, McCormick DA (1993) Cellular mechanisms of a synchronized oscillation in the thalamus. Science 261:361–364. CrossRef Medline

Wafford KA, Thompson SA, Thomas D, Sikela J, Wilcox AS, Whiting PJ (1996) Functional characterization of human gamma-aminobutyric acidA receptors containing the α 4 subunit. Mol Pharmacol 50:670–678. Medline

Wafford KA, van Niel MB, Ma QP, Horridge E, Herd MB, Peden DR, Belelli D, Lambert JJ (2009) Novel compounds selectively enhance δ subunit containing GABA$_A$ receptors and increase tonic currents in thalamus. Neuropharmacology 56:182–189. CrossRef Medline

Wei W, Zhang N, Peng Z, Houser CR, Mody I (2003) Perisynaptic localization of δ subunit-containing GABA$_A$ receptors and their activation by GABA spillover in the mouse dentate gyrus. J Neurosci 23:10650–10661. Medline

Zhang N, Wei W, Mody I, Houser CR (2007) Altered localization of GABA$_A$ receptor subunits on dentate granule cell dendrites influences tonic and phasic inhibition in a mouse model of epilepsy. J Neurosci 27:7520–7531. CrossRef Medline